Tear *N*-glycomics in vernal and atopic keratoconjunctivitis

Angela Messina[1], Angelo Palmigiano[1], Claudia Tosto[1], Donata Agata Romeo[1], Luisa Sturiale[1], Domenico Garozzo[1]*, Andrea Leonardi[2]*

1 Consiglio Nazionale delle Ricerche (CNR), Istituto per i Polimeri, Compositi e Biomateriali, (IPCB) Catania, Italy
2 Department of Neuroscience, Ophthalmology Unit, University of Padua, Italy

Short title: tear glycomics in VKC and AKC

Abstract Word Count: 250
Text Word Count: 3609
Commercial relationship: Authors have no conflict of interest
Source of Funding: This work was partially supported by a generous donation from the "Stella Lucente" trust

Correspondence: Andrea.leonardi@unipd.it and Domenico.garozzo@cnr.it

Corresponding Authors:
Andrea Leonardi, MD
Department of Neuroscience, Ophthalmology Unit, University of Padua
via Giustiniani 2
35128 Padua, Italy
Fax: +39-049-875 5168
email: andrea.leonardi@unipd.it

ABSTRACT

Purpose

Tear fluid *N*-Glycome from patients affected with vernal (VKC) and atopic keratoconjunctivitis (AKC) was investigated to identify specific changes in tears and to recognize possible glyco-biomarkers.

Methods

The analysis of the *N*-glycans was performed using matrix-assisted laser desorption ionization mass spectrometry on single tear samples. Tears from control normal subjects (CTRL), VKC and AKC patients were processed and treated with peptide N-glycosidase F (PNGase F) to deglycosylate *N*-glycoproteins. Released *N*-glycans were purified, permethylated and analyzed by Matrix-Assisted Laser Desorption/Ionization-Time Of Flight Mass Spectrometry and tandem Mass Spectrometry (MALDI-TOF MS and MALDI-TOF MS/MS).

Results

More than 150 complex *N*-glycans, including highly fucosylated biantennary, triantennary, tetraantennary and bisecting species, were observed in our spectra. Three distinct patterns for CTRL, VKC and AKC patients were identified in terms of relative intensities for some *N*-glycans structures. Major variations involved bisecting and hyperfucosylated glycoforms.

The most intense ions were associated to species at *m/z* 1907.0 (asialo, agalacto, bisected, biantennary structure – NGA2B) in CTRL MS profiles, at *m/z* 2605.3 and 2966.5 in VKC, and at *m/z* 2792.4 in AKC corresponding to a well-known biantennary, disialylated *N*-glycan. Several peaks were associated to structures bearing one or two Lewis X epitopes. Structures were confirmed by MS/MS analysis. Quantitative differences among the three groups were statistically significant.

Conclusions

Tear MS profiles are rich in specific glycoforms, particularly those with a high fucosylation degree, indicating both core and peripheral decoration. Tear *N*-glycome analysis provided important information for a better comprehension of VKC and AKC alterations at the molecular level.

Keywords: Glycomics, vernal keratocojunctivitis, atopic keratoconjunctivitis, tears, mass spectrometry

INTRODUCTION

The ocular tear film is a complex mixture of ions, small molecules, glycoproteins and hundreds of proteins, many of which are bioactive [1,2]. The functions of the tear film consist of covering and wetting the surface of the cornea and the conjunctiva, maintaining their integrity, protecting against microbial challenge and preserving the visual acuity. A number of studies reported on differential proteomic analysis of tear fluids of healthy subjects and patients as an approach successfully employed for biomarker search and identification in dry eye disease [3,4], in climatic droplet keratopathy [5], in glaucoma [6] and in vernal keratoconjunctivitis (VKC) [7]. More recently, an increasingly growing interest in glycomic studies has emerged, since qualitative and quantitative glycan alterations are often crucial to afford key information on pathological mechanisms in a large variety of disorders and severe diseases such as rheumatoid arthritis [8,9], diabetes [10], inflammation [11], tumors [12] and Alzheimer's disease [13-19].

Glycosylation is a complex post-translational modification of proteins, very sensitive to the biochemical environment, depending on the action of several glyco-enzymes. Even though it is not under direct genetic control, glycosylation affects several biological processes [20,21].

Glycosylation is an important factor in regulating the ocular surface homeostasis [22]. It was reported that inflammatory stress causes *N*-glycan processing deficiency in ocular autoimmune disease [23], while tear fluid *N*-glycosylation can provide specific and sensitive methods for biomarker discovery and disease diagnosis [24,10]. These pioneering works on tear glycomics suggested a reduced *N*-glycans fucosylation degree as potential biomarker for rosacea [24], and significant quantitative changes in some *N*-glycans in diabetes patients compared to diabetic retinopathy [10]. Both studies reported the identification of about 50 *N*-glycan species, pinpointing structures containing up to seven fucoses by Matrix-Assisted Laser Desorption Ionization Time of Flight Mass Spectrometry (MALDI TOF MS) [24], and complex *N*-glycans carrying up two sialic acids detected by Electrospray Mass Spectrometry (ESI-MS) [10]. Despite these achievements, a complete *N*-glycans profile of tear fluid is still missing because such investigations were performed on free (underivatized) glycans, undergoing sialic acids loss and fucose fragmentation when analyzed by MALDI MS and ESI MS, respectively. Nevertheless, such instances did not affect the aforesaid outcomes, as the analyses by MALDI MS dealt with the identification of *N*-glycan hyperfucosylated structures, while the research handled by ESI MS mainly pointed to extend the characterization of *N*- and *O*-linked sialylated species.

To acquire the human tear fluid *N*-glycoprofile without any loss of information, we carried out MALDI MS analysis on permethylated *N*-glycans, a widely known glycomic approach allowing a high-sensitivity analysis of oligosaccharide species avoiding glycosidic linkage fragmentation. In

the present study we moreover applied the MALDI MS and MS/MS approach to deeply characterize and compare the *N*-linked glycan profiles of tear fluid from normal subjects and from patients affected by VKC and atopic keratoconjunctivitis (AKC), aiming at identifying changes and, possibly, specific glycan features (glyco-biomarkers) associated to these ocular diseases.
VKC and AKC are two severe and persistent types of ocular allergy affecting the conjunctiva and the cornea, impairing the physiology and the function of the ocular surface and possibly causing significant complications leading to vision loss [25]. VKC is a chronic bilateral conjunctival inflammation typically occurring in areas with tropical and temperate climates and with a significant male preponderance, affecting mostly children and young adults [26]. AKC is a bilateral conjunctival and eyelid inflammation, which should be considered the ocular localization of atopic dermatitis [27]. Both VKC and AKC have a characteristic ropey, stringy mucous and/or serous discharge, and possible corneal complications, such as superficial punctate keratopathy (SPK), macroerosions and ulcers. If inappropriately treated, both VKC and AKC can lead to severe complications such as glaucoma, corneal scarring, and blindness. To date, no specific laboratory tests are suitable for VKC and AKC diagnosis and monitoring.

METHODS

Subjects and tear collection

The research followed the Tenets of the Declaration of Helsinki. Institutional Review Board approval was obtained. Written informed consent was obtained from all subjects or, in the case of minors, from their parents after explaining of the nature and the possible consequences of the study. Eleven normal control subjects (CTRL) (5 females, 6 males; mean age 19+5.3; range 7-30), 23 active, consecutive VKC patients (6 females, 17 males; mean age 15±10.4; range 5-40) and 7 active, consecutive AKC patients (4 females, 3 males; mean age 16±4.1; range 8-20) were included in the study (supplementary Table 1). As inclusion criteria, patients were required to have already the diagnosis of VKC and AKC based on typical history, signs and symptoms [26]. A clinical grading of the disease was given using the Bonini's scale [26]. All patients and CTRL were free of medication for at least 5 days before sample collection. Patients were excluded if they demonstrated any active ocular infection or any ocular surface anomaly other than VKC and AKC. Tears were gently collected from the external canthus in the morning between 9am and 11am using a glass Pasteur capillary tube, avoiding the tear reflex as much as possible. Tear samples were centrifuged, supernatants were collected and immediately frozen at -80°C before analysis. Samples were not pooled from both eyes or from different patients.

Sample preparation

Eight µL of tears from CTRL, VKC and AKC patients were diluted 1/10 in a 0.1 % denaturant solution of RapiGest™ (Waters Corporation, Milford, Massachusetts) in 50 mM NH_4HCO_3. Denaturated (glyco)proteins were reduced by adding 100 mM dithiothreitol (DTT) in 50 mM NH_4HCO_3 (final concentration 5 mM) and incubated for 30 min at 56°C. Subsequently, cysteine alkylation was achieved by an addition of 100 mM iodoacetic acid (IAA) in 50 mM NH_4HCO_3 (final concentration 15 mM) and incubation for 40 min at room temperature in the dark. The *N*-linked glycans were enzymatically released by the action of peptide-N-glycosidase F (PNGase F, from Flavobacterium meningosepticum EC 3.5.1.52; Roche Diagnostics GmbH) (2 ml corresponding to 2 units) at 37°C overnight and then purified by solid-phase extraction using Hypercarb cartridges (Thermo Fisher Scientific, Bellefonte, USA). PNGase F treatment is highly efficient in these conditions [28].

Glycan permethylation was afforded as previously described [29] according to Ciucanu and Kerek protocol [30], to further enhance detection sensitivity upon MS investigation. Permethylated *N*-glycans were then subjected to MS investigation by MALDI TOF MS and MALDI TOF/TOF MS/MS to achieve a detailed structural elucidation of some *N*-glycans and univocally establish their structures.

MALDI TOF MS and MS/MS analysis

A few microlitres of permethylated *N*-glycan samples, resuspended in MeOH, were mixed with the same volume of matrix solution (10 mg/ml 5-Chloro-2-mercaptobenzothiazole, CMBT in MeOH/H_2O 80/20). MALDI TOF and MALDI TOF/TOF mass spectra were recorded in reflectron positive mode using a 4800 MALDI TOF/TOF™ (Applied Biosystems) instrument, equipped with an Nd:YAG laser at 355-nm and 200 Hz repetition rate. In MS mode, 1200 shots were accumulated for each spectrum, with a resolution greater than 15K and a mass accuracy better than 80 ppm. The instrument parameters employed for the MS and MS/MS analyses are reported in supplementary Table 2 and supplementary Table 3. A 4700-calibration standard kit, calmix (Applied Biosystems) was used as the external calibrant for the MS mode, and [Glu1] fibrinopeptide B human (Sigma) was used as the external calibrant for the MS/MS mode (1 µL of TOF/TOF Calibration Mixture in 24 µL of CHCA matrix solution).

The MS data were processed by DataExplorer™ 4.9 software and the *N*-glycan species were identified by bioinformatics tools, such as GlycoMod (http://web.expasy.org/glycomod/),

Glycoworkbench v2.1 [31] and by tools provided by the Consortium for Functional Glycomics (CFG).

All the MS/MS spectra recorded, and some of the MALDI TOF mass spectra of permethylated N-glycans released by PNGase F from CTRL, VKC and AKC patients can be downloaded from www.ipcb.ct.cnr.it/ct/spectraVisualizza.jsp

Tear serotransferrin quantitative analysis

Tears from the 7 AKC and 7 VKC patients,, and from 7 CTRL were used to measure tear concentrations of serotransferrin by the commercial quantitative immunochemical analysis (Dimension Vista System, Siemens, Erlangen, Germany) (Limit of Detection (LOD) is 0.002 mg/L).

Statistical analyses

Statistical analyses were accomplished using a commercially available software program (PASW Statistics 18). Specificity and relevance of quantitative differentiations were established by ANOVA p-values and results were expressed as mean values ± SD (standard deviation). In relation to serotransferrin tear levels, since none of the groups showed a normal distribution (Shapiro-Wilk's test $p<0.05$), sample values were expressed by median ± interquartile range (IRQ). Comparison among groups was performed by the U Mann-Whitney test with normal approximation and 0.5 continuity correction. For statistical significance, the threshold p value was $p\leq0.05$.

RESULTS

***N*-glycosylation analysis of control tear fluid**

Tear samples from the 11 CTRL were processed as described and analyzed by MALDI TOF MS in order to define the typical tear *N*-glycan pattern in healthy subjects. Permethylated glycans were detected in positive polarity as Na^+ ion adducts, whose molecular masses differ from their theoretical protonated counterpart by 22 amu (atomic mass unit). All the CTRL mass spectra were found to be very similar to the profile in Figure 1A (supplementary Figure S1), showing more than 150 peaks corresponding to $[M + Na]^+$ pseudo-molecular ions from *m/z* 1579.8 to *m/z* 4432.2 (supplementary Table 4). Spectra showed the occurrence of a wide range of *N*-glycans categories including oligomannose, complex bi-, tri-, and tetra-antennary, neutral, acidic, bisected and hybrid

species. Additionally, the main peaks were further analyzed by MALDI TOF/TOF MS/MS. This analysis was crucial to discriminate, in most cases, between isomeric glycoforms or to confirm the presence of 2 or even more isomeric glycoforms associated to a single molecular mass.

Oligomannose N-glycans

Peaks related to oligomannose glycans were observed in Figure 1A (supplementary Figure S1) at *m/z* 1579.8 (Man5), 1783.9 (Man6), 1988.0 (Man7), 2192.1 (Man8). The MS/MS spectra (supplementary Figures S4, S5, S6, S7), confirmed these assignments.

Mono-, di- and multi-fucosylated N-glycans

Amongst the *N*-glycan structures (approximately 150) listed in supplementary Table 4, 116 (about 75%) were fucosylated, being 41 out of 116 mono-fucosylated and 75 out of 116 bearing more than 1 fucose unit, with 2 glycans having up to 7 fucose moieties. Core fucosylated and peripheral fucosylated *N*-glycans, depending on fucose localization, were both present in the CTRL tear *N*-glycome profile. In the present study, core fucosylation (due to an α1-6 fucose linked to the *N*-acetylglucosamine bound to the protein), and peripheral fucosylation, (due to a fucose moiety 1-3 or 1-4 linked to an antennary N-acetylglucosamine or 1-2 linked to a galatose [32]) were characterized by the occurrence of specific MS/MS ions. Antennary fucosylation allowed us to recognize specific epitopes belonging to the Lewis (Le) family (structural features typical of blood group antigens [33]) (see supplementary Table 5).

Core fucosylated glycans and/or *N*-glycans bearing $Le^{x/a}$, $sLe^{x/a}$ or $Le^{y/b}$ motifs were identified (current approaches based MALDI MS and MS/MS on permethylated *N*-glycans do not provide informations on linkage positions, in order to discriminate (s)Le^a from (s)Le^x and Le^b from Le^y). The occurrence of a $Le^{x/a}$ epitope was confirmed by the ion at *m/z* 660.3 in the fragmentation spectra of the glycan strucures at *m/z* 2418.2, 2592.3, 2605.3, 2766.4 and 2779.4. Figure 2 shows the MS/MS spectrum of the latter peak, whereas the other fragmentation spectra are reported in the supplementary (supplementary Figures S8, S9, S10, S11). MS/MS analysis allowed us to identify some ions corresponding to more than one isomeric structure (i.e., peak at *m/z* 2605.3 in Figure S10 is actually related to a mixture of 2 glycans, a core fucosylated one and a second bearing a $Le^{x/a}$ epitope).

The $sLe^{x/a}$ motif, recognized through the fragment at *m/z* 1021.5, was associated to the glycan structures at *m/z* 3127.6, 3140.6 and 3589.8 (supplementary Figures S12, S13, S14). Interestingly, the structure at *m/z* 3127.6 corresponded to a glycoform owning 4 fucoses, suggesting that in the core fucose, $sLe^{x/a}$ and $Le^{y/b}$ epitopes are present in the same glycan (supplementary Figure S12).

Le^y (and/or Le^b) pattern is proven by the fragment at *m/z* 834.4 occurring in the fragmentation spectra of the glycans at *m/z* 2418.2, 2592.3, 2766.4, 2940.5 and 3127.6 (see Figures S8, S9, S11, S15 and S12 respectively).

Bisected N-glycans

A number of complex structures with bisecting GlcNAc were present in CTRL tear fluid profiles, including 2 very intense ions at *m/z* 1906.9 and 2081.1 that correspond to the agalactosyl-biantennary structure A2B and to the same structure core fucosylated (FA2B), respectively. Since permethylated bisected species showed no characteristic fragments by MALDI MS/MS, structural characterization was achieved by comparing the fragmentation spectra with the model compound as already reported [13].

Sialylated N-glycans

A large portion of the identified tears *N*-glycans bore a sialic acid as terminal antennary residue. Diagnostic fragments observed by MS/MS are *m/z* 847.4 corresponding to the sialylated lactosamine epitope or *m/z* 1021.5 corresponding to the fucosylated homologous ($sLe^{x/a}$ motif).

Hybrid glycans

A minor component of hybrid glycans was also detected. MS/MS analysis confirmed that peaks at *m/z* 2156.1 (supplementary Figure S16) and 2360.2 (supplementary Figure S17) corresponded to hybrid structures with terminal sialic acid and core fucosylation.

Tears *N*-glycosylation of VKC patients

MALDI -TOF *N*-glycans analyses were performed in 23 VKC individual tear samples. A uniquely distinctive profile emerged from these patients (Figure 1B, supplementary Figure S2). Peaks at *m/z* 2605.3 and 2966.5 corresponded to biantennary monofucosylated structures bearing 1 and 2 sialic acids respectively, whereas the ions at *m/z* 3415.7 and 3776.9 matched monofucosylated triantennary structures bearing 2 and 3 sialic acids respectively. These 2 structures showed the fucose unit linked either to the chitobiose core or to the antennary *N*-acetylglucosamine. Interestingly, the ion at *m/z* 2792.4, related to the biantennary disialo structure, was more intense in VKC patients compared to CTRL (Figure 1A, supplementary Figure S1). On the contrary, peaks corresponding to truncated *N*-glycans at *m/z* 1907.0, 2081.0 and 2285.1 were 2- or 3-fold less intense than the corresponding ones in the CTRL. Statistical differences between VKC and CTRL in relative intensities of the peaks are shown in Figure 3A. Interestingly, in VKC glyco-profiles the ions corresponding to the sialylated structures are more abundant, whereas, in the bisected *N*-glycan series they are less abundant. No specific patterns were identified dividing VKC patients by age or gender. The levels of the selected glycans were not correlated with the clinical score of the disease.

Tear *N*-glycosylation of AKC patients

All tears samples from the 7 AKC patients showed similar glyco-profiles (Figure 1C, supplementary Figure S3). Compared to CTRL and VKC, AKC spectra showed a strong increase of the species at *m/z* 2431.2 and 2792.4 (corresponding to biantennary *N*-glycans carrying 1 and 2 sialic acids respectively) and also a decrease of the ions at m/z 2605.3 and m/z 2966.5 associated to their fucosylated counterparts. Minor increase of the *N*-glycans corresponding to the sialylated triantennary series (*m/z* 3602.8 and *m/z* 3776.9) was detected. Furthermore, a significant increase of oligomannose and bisected species besides a decrease of sialylated species, with the exception of the peak at *m/z* 2953.5, was observed (Figure 3B). Significant ($p < 0.01$) differences in glycans intensities between AKC and VKC patients were also present (supplementary Figure S18). No specific patterns were identified dividing AKC patients by age or gender. The levels of the selected glycans were not correlated with the clinical score of the disease.

Tear serotransferrin quantitative analysis

Quantitative analysis of serotransferrin, associated to the peak at *m/z* 2792.4, confirmed the significant increase of this protein in AKC and VKC tears compared to CTRL ($p=0.0014$) and higher levels in AKC compared to VKC ($p=0.0039$) (Figure 4).

DISCUSSION

MALDI-MS profiling and MALDI-MS/MS characterization of permethylated *N*-glycans permitted to extend the repertoire of the identified *N*-glycans in the normal control tear fluid up to $\simeq$ 150, as reported in Table S4. Many of the glycans shown in the table were detected for the first time because, as already mentioned in the introduction, MALDI analysis of underivatized glycans underestimates the amount of sialylated glycans, and ESI-MS underestimates the occurrence of structures decorated with fucose units. Conversely, MALDI MS of permethylated glycans is an effective method to detect both of these *N*-glycan series. Although this approach does not allow to trace the proteins from which the identified glycans originated, it is important to highlight that two glycoproteins were found more abundant in the normal tear fluid than others [34]: lactoferrin (1.56 g/L) and secretory Immunoglobulin A (sIgA) (2.07 g/L). Another major glycoprotein certainly contributing to the overall glycosylation profile is Immunoglobulin G (IgG), which is present in

tears at a much lower concentration (0.004 g /L) [34]. The *N*-glycosylation of lactoferrin and sIgA has been extensively studied [35,36]. We believe that oligomannose and asymmetrically branched *N*-glycans originate mostly from lactoferrin, complex-type glycans (mainly biantennary and bisected) which derive predominantly from IgA monomers, multi-fucosylated glycans from the Secretory Component of IgA, and monoantennary and hybrid-type glycans from the joining chain of secretory IgA.

All the obtained tear MS profiles were rich in specific glycoforms, particularly those with a high fucosylation degree, indicating both core and peripheral decoration, these last essential components of antigens belonging to the Lewis family on the cell membrane surface. Increased levels of fucosylation have been implicated in several diseases: a) inflammatory diseases, since *N*-glycans fucosylation plays a regulatory role for selectin-dependent leukocyte adhesion [37]; b) immunological response, due to the regulatory role of fucosylated glycoforms in immune response and to the autoimmunity development [38,39]; c) cancer, promoting TNF-α activity in M1 inflammatory macrophages [40].

Large differences emerged from the comparison of *N*-glycome profiles from control, VKC and AKC tear fluids. In control samples, the base peak was the bisected specie at *m/z* 1907.0. In VKC, dominant ions were assigned to the biantennary and core fucosylated glycans at *m/z* 2605.3 and *m/z* 2966.5. The AKC MS profiles showed a huge increase of the ion at *m/z* 2792.4, (biantennary, disialylated unfucosylated glycoform), with respect to CTRL and VKC tears. These glycomic data are in agreement with our previous results on quantitative proteomics of VKC tears, which showed the increase of serotransferrin and lactotransferrin with a concomitant reduction of immunoglobulins [7]. These results suggest that the peaks with increased intensities can be referred to glycans from lactotransferrin (*m/z* 2966.5 and 2605.3) [36,41,42] and from serotransferrin (*m/z* 2792.4) [29,43], whereas peaks with decreased intensity may be associated to immunoglobulins. Serotransferrin is an iron-binding plasma glycoprotein, primarily expressed in the liver but also in corneal epithelial cells [44]. It has been shown that patients with allergy and allergic keratoconjunctivitis suffer an increased oxidative stress condition [45,46]. The capacity of binding free iron to protect against toxic radical oxygen species gives to the serotransferrin an antioxidant effect inhibiting iron-mediated oxidation [45]. Serotransferrin, usually present in tears in very low concentrations, belongs to the ocular innate immune system and contributes, along with lactoferrin, to the iron-sequestration mechanisms against pathogens. Serotransferrin and other serum proteins not commonly present at high levels on the ocular surface (such as albumin and IgG), may presumably derive from plasma through blood vessel passive filtration. Their presence in the tear film could be due to a serum leakage in response to ocular inflammation, to a stimulation of the

conjunctiva or to a mild ocular trauma [47]. However, the dramatic increase of the typical serum glycoform at *m/z* 2792.4 and the relatively reduced intensity of peaks related to immunoglobulins in VKC and AKC MS profiles, combined with the high serotransferrin tear levels in AKC and, in lesser extent, in VKC, may suggest a local production of serotransferrin in addition of serum leakage due to the ocular inflammation. A reduction in serotransferrin tear levels has been shown in a rabbit model of Sjögren syndrome-associated dry eye [48] and in saporin toxin denervated lacrimal glands rat-model despite normal tear production [49]. Differently from dry eye, ocular allergy is characterized by increased tearing and corneal sensitivity, and by corneal nerve fiber abnormalities [50,51]. The antimicrobial, antiviral, antiparasitic and anti-inflammatory activity of serotransferrin and of other over-expressed tear fluid proteins may explain the low rate of infection in ocular allergy patients and may function as an up-regulating mechanism to down-regulate the effects of pro-inflammatory cytokine overexpressed by the allergic reaction [52].

Several inflammatory diseases associated with altered levels of sIgA and serum IgA have been found [53]. In ocular allergy, tear sIgA concentration have been reported to be reduced in VKC, AKC and perennial allergic conjunctivitis (PAC) compared to normal subjects [54], whereas serum IgA are usually elevated in Sjögren's syndrome as a result of a reduced hepatocyte clearance due to increased IgA glycan sialylation [55-57]. N-glycosylation plays also an important role in allergy and in antibody-dependent cell mediated cytotoxicity (ADCC) [35,58]. In fact, bisected structures are known to promote the IgG binding affinity towards cristallizzable fragment receptors (FcR) of effector immune cells, thus enhancing ADCC. On the contrary, core fucosylation enhances cytotoxicity by reducing antibody affinity for FcR. [55,59,60,61]. Similarly, sialylated and galactosylated structures have an anti-inflammatory effect, whereas agaloctosylated structures are recognized as pro-inflammatory [55,59,60]. Moreover, it was recently reported that sialylation of IgE is a determinant of allergic pathology [62] In fact, removal of sialic acid from IgE attenuated effector-cell degranulation and anaphylaxis in several functional models of allergic disease [62]. In the present work, all the major N-glycan structures bearing bisecting GlcNAc (i.e. the species at *m/z* 1907.0, 2081.0, 2111.0 and 2285.1 in Figure 3) are under-represented in VKC and AKC tears, probably due to sIgA reduction, as reported in VKC and AKC patients [54]. Conversely, the high-fucosylated bisected species at *m/z* 2837.4 and 3024.5, are over-expressed. This suggests that, in addition to the decrease of sIgA levels in VKC and AKC tears, a concomitant change in N-glycosylation of the secretory component which may impact the sIgA interactions with the local environment [63].

In conclusion, we identified in normal control tears multiple specific glycoforms, many of whom with a high fucosylation degree. Tear *N*-glycome analysis highlighted profound and specific changes of tear proteome and N-glycome in allergic keratoconjunctivitis compared to control tears.

Funding

This work was partially supported by a generous donation from the “Stella Lucente” trust

Disclosure/Conflict of Interest statement

The authors declare no conflicts of interest

Figure legends

Fig. 1. MALDI TOF mass spectra, with major assignments, of permethylated *N*-glycans released by PNGase F from control (CTRL) (A), vernal keratoconjunctivitis (VKC) (B) and atopic keratoconjunctivitis (AKC) (C) tears.
N-acetylglucosamine (GlcNAc): blue square; Mannose (Man): green circle; Galactose (Gal): yellow circle; Sialic acid (NeuAc): purple lozenge; Fucose (Fuc): red triangle.

Fig. 2. MALDI TOF/TOF fragmentation analysis of the parent ion at *m/z* 2779.4 present in the MS spectra from a control tear.
N-acetylglucosamine (GlcNAc): blue square; Mannose (Man): green circle; Galactose (Gal): yellow circle; Sialic acid (NeuAc): purple lozenge; Fucose (Fuc): red triangle.

Fig. 3. Comparison of statistically significant relative intensities between control subjects (CTRL) and vernal keratoconjunctivitis (VKC) patients (A), CTRL and atopic keratoconjunctivitis (AKC) patients (B). Most intense 30 peaks were compared and only statistically significant are shown. Bars indicate standard errors (*$p<0.01$; **$p<0.001$).

Fig. 4. Tear levels of serotransferrin, by commercial immunometric analysis, in the cohort of atopic keratoconjunctivitis (AKC) and vernal keratoconjunctivitis (VKC) patients and control subjects (CTRL). Tear levels were significantly higher in AKC and VKC compared to CTRL, and in AKC compared to VKC (p-values by U Mann-Whitney test).

Supplementary figure Legends

Figures S1-S3: MALDI TOF mass spectra, with major assignments, of permethylated *N*-glycans released by PNGase F from control (CTRL) (S1), vernal keratoconjunctivitis (VKC) (S2) and atopic keratoconjunctivitis (AKC) (S3) tears.

Figures S4-S17: MALDI-TOF/TOF fragmentation analysis of the parent ion at *m/z* 1579.8, *m/z* 1783.9, *m/z* 1988.0, *m/z* 2192.1, *m/z* 2418.2, *m/z* 2592.3, *m/z* 2605.3, *m/z* 2766.4, *m/z* 3127.6, *m/z* 3140.6, *m/z* 3589.8, *m/z* 2940.5, *m/z* 2156.1, *m/z* 2360.2 respectively, present in the mass spectrum from a CTRL tear. MS/MS spectra recorded in several samples including VKC and AKC showed no differences.

N-acetylglucosamine (GlcNAc): blue square; Mannose (Man): green circle; Galactose (Gal): yellow circle; Sialic acid (NeuAc): purple lozenge; Fucose (Fuc): red triangle.

Figure S18: Comparison of statistically significant relative intensities between vernal keratoconjunctivitis (VKC) patients and atopic keratoconjunctivitis (AKC) patients. Only statistically significant glycans are shown.

Acknowledgments.

a. Funding/Support: This work was partially supported by a generous donation from the “Stella Lucente” trust

b. Conflicts of Interest:
Angela Messina: No Conflicts of Interest
Angelo Palmigiano: No Conflicts of Interest
Claudia Tosto: No Conflicts of Interest
Donata Agata Romeo: No Conflicts of Interest
Luisa Sturiale: No Conflicts of Interest
Domenico Garozzo: No Conflicts of Interest
Andrea Leonardi: No Conflicts of Interest.

c. Contributions to Authors in each of these areas: Angela Messina (AM), Angelo Palmigiano (AP), Claudia Tosto (CT), Donata Agata Romeo (DAR), Luisa Sturiale (LS), Domenico Garozzo (DG), Andrea Leonardi (AL)
Conception and Design: AL, DG, AM
Analysis and interpretation: DG, AL, AM, LS, AP
Writing the article: AM, AL, DG, LS
Critical revision of the article: LS, DAR, CT
Final approval of the article: AL, SD, JLF, LD, SD, DR, MK
Data Collection: AM, AP, CT, DAR, LS, DG, AL
Provision of materials, patients, or resources: AL, DG
Statistical expertise: LS, CT
Obtaining funding: DG
Literature search: AM, AL, DG, LS,
Administrative, technical or logistic support: AL, DG, AP
d. Statement about Conformity with Author Information: none
e. Other Acknowledgments: none

References

1. Zhou L, Zhao SZ, Koh SK, Chen L, Vaz C, Tanavde V et al. In-depth analysis of the human tear proteome. J Proteomics 2012;75:3877-85.

2. de Souza GA, Godoy LM, Mann M. Identification of 491 proteins in the tear fluid proteome reveals a large number of proteases and protease inhibitors. Genome Biol 2006;7:R72.

3. Zhou L, Beuerman RW, Chan CM, Zhao SZ, Li XR, Yang H et al. Identification of tear fluid biomarkers in dry eye syndrome using iTRAQ quantitative proteomics. J Proteome Res 2009;8:4889-905.

4. Tong L, Zhou L, Beuerman RW, Zhao SZ, Li XR. Association of tear proteins with Meibomian gland disease and dry eye symptoms. Brit J Ophthalmol 2011;95(6):848-52.

5. Lei Z, Beuerman RW, Chew AP, Koh SK, Cafaro TA, Urrets-Zavalia EA et al. Quantitative analysis of *N*-linked glycoproteins in tear fluid of climatic droplet keratopathy by glycopeptide capture and iTRAQ. J Proteome Res 2009;8:1992-2003.

6. Wong TT, Zhou L, Li J, Tong L, Zhao SZ, Li XR, et al. Proteomic profiling of inflammatory signaling molecules in the tears of patients on chronic glaucoma medication. Invest Ophth Vis Sci 2011;52(10):7385-91.

7. Leonardi A, Palmigiano A, Mazzola EA, Messina A, Milazzo EMS, Bortolotti M et al. Identification of human tear fluid biomarkers in vernal keratoconjunctivitis using iTRAQ quantitative proteomics. Allergy 2014;69(2):254-56.

8. Parekh RB, Dwek RA, Sutton BJ, Fernandes DL, Leung A, Stanworth D et al. Association of rheumatoid arthritis and primary osteoarthritis with changes in the glycosylation pattern of total serum IgG. Nature 1985;316(6027):452-57.

9. Parekh R, Roitt I, Isenberg D, Dwek R, Rademacher T. Age-related galactosylation of the *N*-linked oligosaccharides of human serum IgG. J Exp Med 1988;167(5):1731-36.

10. Nguyen-Khuong T, Everest-Dass AV, Kautto L, Zhao Z, Willcox MD, Packer NH. Glycomic characterization of basal tears and changes with diabetes and diabetic retinopathy. Glycobiology 2015;25(3):269-83.

11. Wang J, Yang D, Li C, Shang S, Xiang J. Expression of extracellular matrix metalloproteinase inducer glycosylation and caveolin-1 in healthy and inflamed human gingiva. J Periodontal Res 2014;49(2):197-204.

12. Adamczyk B, Tharmalingam T, Rudd PM. Glycans as cancer biomarkers. Biochim Biophys Acta(BBA)-Gen Subj 2012;1820(9):1347-53.

13. Palmigiano A, Barone R, Sturiale L, Sanfilippo C, Bua RO, Romeo DA et al. CSF *N*-glycoproteomics for early diagnosis in Alzheimer's disease. J Proteomics 2016;131:29-37.

14. Palmigiano A, Messina A, Bua RO, Barone R, Sturiale L, Zappia M et al.: CSF *N*-Glycomics using MALDI MS techniques in Alzheimer's Disease, in Perneczky R (ed): Biomarkers for Alzheimer's Disease Drug Development. New York, NY: Humana Press, 2018, pp. 75-91.

15. Messina A, Palmigiano A, Bua RO, Romeo DA, Barone R, Sturiale L et al.: CSF *N*-Glycoproteomics Using MALDI MS Techniques in Neurodegenerative Diseases, in Santamaria E, Fernandez-Irigoyen J (eds): Cerebrospinal Fluid (CSF) Proteomics. New York, NY: Humana, 2019, pp. 255-72.

16. Kizuka Y, Kitazume S,Taniguchi N. *N*-glycan and Alzheimer's disease. Biochim Biophy Acta (BBA)-General Subjects 2017;1861(10):2447-54.

17. Cho BG, Veillon L, Mechref Y.*N*-Glycan Profile of Cerebrospinal Fluids from Alzheimer's Disease Patients Using Liquid Chromatography with Mass Spectrometry. J Proteome Res 2019;18(10):3770-79.

18. Quaranta A, Karlsson I, Ndreu L, Marini F, Ingelsson M, Thorsén G. Glycosylation profiling of selected proteins in cerebrospinal fluid from Alzheimer's disease and healthy subjects. Anal Methods-UK 2019;11(26):3331-40.

19. Schedin-Weiss S, Gaunitz S, Sui P, Chen Q, Haslam SM, Blennow K, et al. Glycan biomarkers for Alzheimer disease correlate with T-tau and P-tau in cerebrospinal fluid in subjective cognitive impairment. FEBS J 2019.

20. Dwek RA. Glycobiology: toward understanding the function of sugars. Chem Rev 1996;96(2):683-720.

21. Kobata A. A journey to the world of glycobiology. Glycoconjugate J 2000;17(7-9):443-64.

22. Rodriguez Benavente MC, Argüeso P. Glycosylation pathways at the ocular surface. Biochem Soc T 2018;46(2):343-50.

23. Woodward AM, Lehoux S, Mantelli F, Di Zazzo A, Brockhausen I, Bonini S, Argüeso P. Inflammatory stress causes N-glycan processing deficiency in ocular autoimmune disease. Am J Pathol 2019;189(2):283-94.

24. Vieira AC, An HJ, Ozcan S, Kim JH, Lebrilla CB, Mannis MJ. Glycomic analysis of tear and saliva in ocular rosacea patients: the search for a biomarker. Ocul Surf 2012;10(3):184-92.

25. Leonardi A, Doan S, Fauquert JL, Bozkurt B, Allegri P, Marmouz F et al. Diagnostic tools in ocular allergy. Allergy 2017;72(10):1485-98.

26. Leonardi A. Vernal keratoconjunctivitis: pathogenesis and treatment. Prog Retin Eye Res 2002;21:319-39.

27. Hu Y, Matsumoto Y, Dogru M, Okada N, Igarashi A, Fukagawa K et al. The differences of tear function and ocular surface findings in patients with atopic keratoconjunctivitis and vernal keratoconjunctivitis. Allergy 2007;62(8):917-25.

28. Yu YQ, Gilar M, Kaska J, Gebler JC. A rapid sample preparation method for mass spectrometric characterization of N-linked glycans. Rapid Comm Mass Sp 2005;19(16):2331-36.

29. Sturiale L, Barone R, Garozzo D. The impact of mass spectrometry in the diagnosis of congenital disorders of glycosylation. J Inherit Metab Dis 2011;34:891-99.

30. Ciucanu I, Kerek F. A simple and rapid method for the permethylation of carbohydrates. Carbohyd Res 1984;131:209-17.

31. Ceroni A, Maass K, Geyer H, Geyer R, Dell A. Haslam SM. GlycoWorkbench: a tool for the computer-assisted annotation of mass spectra of glycans. J Proteome Res 2008;7:1650-59.

32. Ma B, Simala-Grant JL, Taylor DE. Fucosylation in prokaryotes and eukaryotes. Glycobiology 2006;16(12):158R-184R.

33. Stanley P, Cummings RD: Structures Common to Different Glycans, in: Varki A, Cummings RD, Esko JD et al (eds): Essentials of Glycobiology 3rd edition. Cold Spring Harbor (NY): Cold Spring Harbor Laboratory Press, 2017, pp 161-78.

34. Tiffany JM: Tears and conjunctiva, in Harding JJ (ed.): Biochemistry of the eye. London, Chapman & Hall Medical, 1997, pp. 45-78.

35. Plomp R, de Haan N, Bondt A, Murli J, Dotz V, Wuhrer M. Comparative glycomics of immunoglobulin A and G from saliva and plasma reveals biomarker potential. Front Immunol 2018;9:2436.

36. Karav S, German JB, Rouquié C, Le Parc A, Barile D. Studying lactoferrin *N*-glycosylation. Int J Mol Sci 2017;18(4):870.

37. Li J, Hsu HC, Mountz JD, Allen JG. Unmasking Fucosylation: from Cell Adhesion to Immune System Regulation and Diseases. Cell Chem Biol 2018;25(5):499-512.

38. Bianco GA, Toscano MA, Ilarregui JM, Rabinovich GA. Impact of protein-glycan interactions in the regulation of autoimmunity and chronic inflammation. Autoimmun Rev 2006;5(5):349-56.

39. Lowe JB. Glycan-dependent leukocyte adhesion and recruitment in inflammation. Curr Opin Cell Biol 2003;15(5):531-38.

40. Li J, Hsu HC, Ding Y, Li H, Wu Q, Yang P et al. Inhibition of fucosylation reshapes inflammatory macrophages and suppresses type II collagen-induced arthritis. Arthritis Rheumatol 2014;66(9):2368-79.

41. Barboza M, Pinzon J, Wickramasinghe S, Froehlich JW, Moeller I, Smilowitz JT et al. Glycosylation of human milk lactoferrin exhibits dynamic changes during early lactation enhancing its role in pathogenic bacteria-host interactions. Mol Cell Proteomics 2012;11(6):p. mcp.M111.015248.

42. Le Parc A, Dallas D, Duaut S, Léonil J, Martin P, Barile D. Characterization of goat milk lactoferrin *N*-glycans and comparison with the *N*-glycomes of human and bovine milk. Electrophoresis 2014;35(11):1560-70.

43. Sturiale L, Barone R, Palmigiano A, Ndosimao CN, Briones P, Adamowicz M et al. Multiplexed glycoproteomic analysis of glycosylation disorders by sequential yolk immunoglobulins immunoseparation and MALDI-TOF MS. Proteomics 2008;8(18):3822-32.

44. Kompella UB, Sundaram S, Raghava S, Escobar ER. Luteinizing hormone-releasing hormone agonist and transferrin functionalizations enhance nanoparticle delivery in a novel bovine ex vivo eye model. Mol Vis 2006;12:1185-98.

45. Bakkeheim E, Mowinckel P, Carlsen KH, Burney P, Carlsen KC. Altered oxidative state in schoolchildren with asthma and allergic rhinitis. Pediatr Allergy Immu 2011;22:178-85.

46. Wakamatsu TH, Dogru M, Ayako I, Takano Y, Matsumoto Y, Ibrahim OM et al. Evaluation of lipid oxidative stress status and inflammation in atopic ocular surface disease. Mol Vis 2010;16:2465-75.

47. Fullard RJ, Snyder C. Protein levels in nonstimulated and stimulated tears of normal human subjects. Invest Ophth Vis Sci 1990;31(6):1119-26.

48. Zhou L, Wei R, Zhao P, Koh S K, Beuerman RW, Ding C. Proteomic analysis revealed the altered tear protein profile in a rabbit model of Sjögren's syndrome-associated dry eye. Proteomics 2013;13(16):2469-81.

49. Hegarty DM, David LL, Aicher SA. Lacrimal Gland Denervation Alters Tear Protein Composition and Impairs Ipsilateral Eye Closures and Corneal Nociception. Invest Ophth Vis Sci 2018;59(12):5217-24.

50. Leonardi A, Lazzarini D, Bortolotti M, Piliego F, Midena E, Fregona I. Corneal confocal microscopy in patients with vernal keratoconjunctivitis. Ophthalmology 2012;119(3):509-15.

51. Hu Y, Matsumoto Y, Adan ES, Dogru M, Fukagawa K, Tsubota K et al. Corneal in vivo confocal scanning laser microscopy in patients with atopic keratoconjunctivitis. Ophthalmology 2008;115(11):2004-12.

52. Leonardi A. Allergy and allergic mediators in tears. Exp Eye Res 2013;117:106-17.

53. Mkaddem SB, Christou I, Rossato E, Berthelot L, Lehuen A, Monteiro RC. IgA, IgA receptors, and their anti-inflammatory properties. In Daeron M, Nimmerjahn F (eds): Fc Receptors. Current Topics in Microbiology and Immunology. Springer, Cham., 2014, pp. 221-235.

54. Inada N, Shoji J, Hoshino M, Sawa M. Evaluation of total and allergen-specific secretory IgA in tears of allergic conjunctival disease patients. Jpn J Ophthalmol. 2007;51(5):338-42.

55. Arnold JN, Wormald MR, Sim RB, Rudd PM, Dwek RA. The impact of glycosylation on the biological function and structure of human immunoglobulins. Annu Rev Immunol 2007;25:21-50.

56. Basset C, Durand V, Jamin C, Clement J, Pennec Y, Youinou P, Dueymes M, Roitt IM. Increased N-linked glycosylation leading to oversialylation of monomeric immunoglobulin A1 from patients with Sjögren's syndrome. Scand J Immunol 2000;51(3):300-6.

57. Rifai A, Fadden K, Morrison SL, Chintalacharuvu KR. The N-glycans determine the differential blood clearance and hepatic uptake of human immunoglobulin (Ig) A1 and IgA2 isotypes. J Exp Med 2000;191(12):2171-82.

58. Royle L, Roos A, Harvey DJ, Wormald MR, Van Gijlswijk-Janssen D, Redwan ER, Wilson IA, Daha MR, Dwek RA, Rudd PM. Secretory IgA N-and O-glycans provide a link between the innate and adaptive immune systems. J Biol Chem 2003;278(22):20140-53.

59. Jennewein MF, Alter G. The immunoregulatory roles of antibody glycosylation. Trends Immunol 2017;38(5):358-72.

60. Gudelj I, Lauc G, Pezer M. Immunoglobulin G glycosylation in aging and diseases. Cell Immunol 2018;333:65-79.

61. Umaña P, Jean–Mairet J, Moudry R, Amstutz H, Bailey JE. Engineered glycoforms of an antineuroblastoma IgG1 with optimized antibody-dependent cellular cytotoxic activity. Nat Biotechnol 1999;17(2):176-80.

62. Shade KT, Conroy ME, Washburn N, Kitaoka M, Huynh DJ, Laprise E, Patil SU, Shreffler WG, Anthony RM. Sialylation of immunoglobulin E is a determinant of allergic pathogenicity. Nature 2020;582:265-70.

63. Phalipon A, Cardona A, Kraehenbuhl JP, Edelman L, Sansonetti PJ, Corthésy B. Secretory component: a new role in secretory IgA-mediated immune exclusion in vivo. Immunity 2002;17(1):107-15.

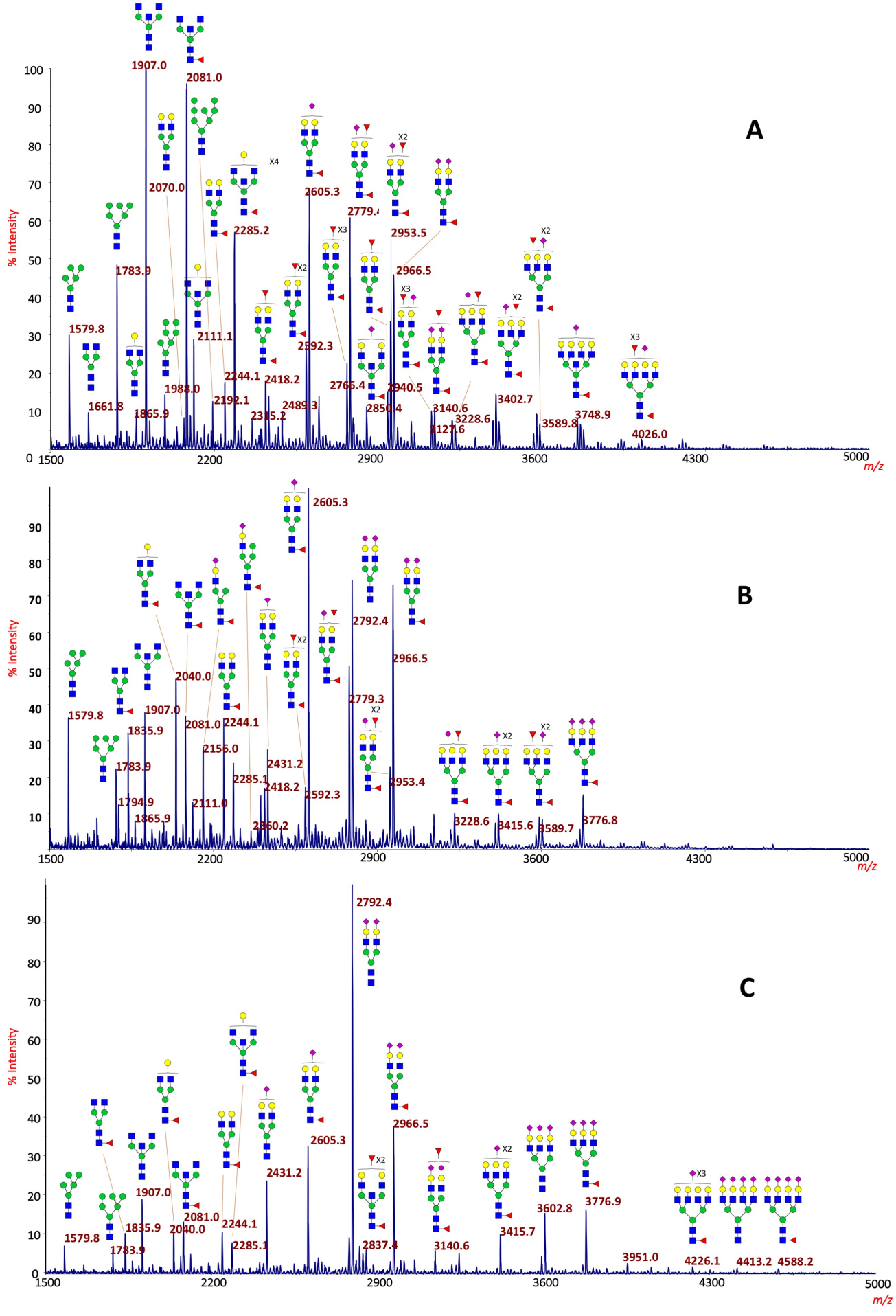
A
% Intensity
m/z
1907.0
2081.0
2070.0
2285.2
2605.3
2779.4
2953.5
2966.5
1783.9
1579.8
2111.1
2892.3
2244.1
2418.2
1988.0
2192.1
2765.4
2940.5
1661.8
1865.9
2489.3
2315.2
2850.4
3140.6
3228.6
3127.6
3402.7
3589.8
3748.9
4026.0
B
2605.3
2792.4
2966.5
2040.0
2779.3
1579.8
1907.0
2081.0
2244.1
1835.9
2156.0
2431.2
1783.9
2285.1
2418.2
2953.4
2592.3
1794.9
2111.0
1865.9
2360.2
3228.6
3415.6
3589.7
3776.8
C
2792.4
2966.5
2605.3
2431.2
1907.0
2081.0
2040.0
2244.1
1835.9
1579.8
2285.1
1783.9
2837.4
3140.6
3415.7
3602.8
3776.9
3951.0
4226.1
4413.2
4588.2

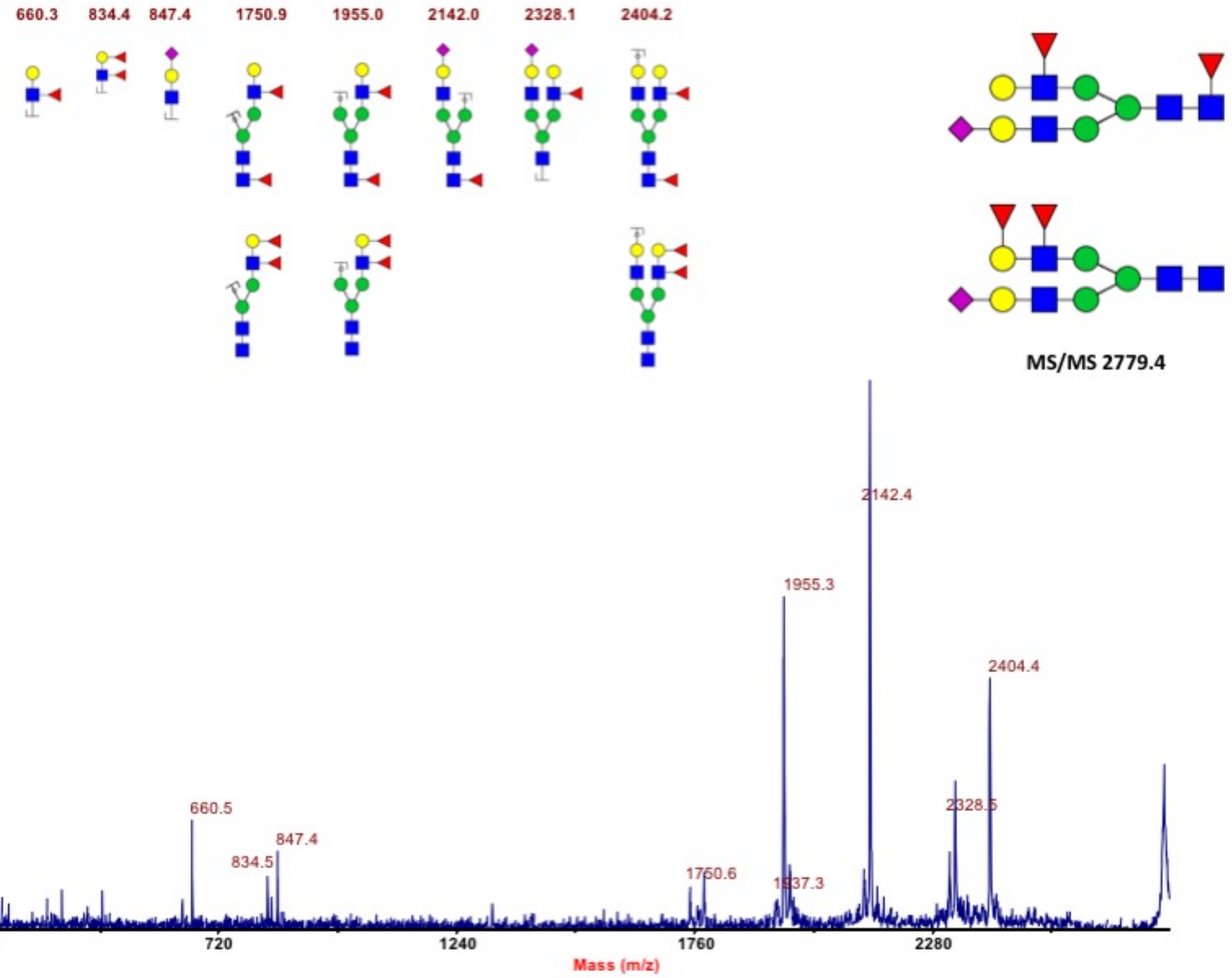
660.3
834.4
847.4
1750.9
1955.0
2142.0
2328.1
2404.2
MS/MS 2779.4
% Intensity
Mass (m/z)
660.5
834.5
847.4
1750.6
1837.3
1955.3
2142.4
2328.5
2404.4
200
720
1240
1760
2280

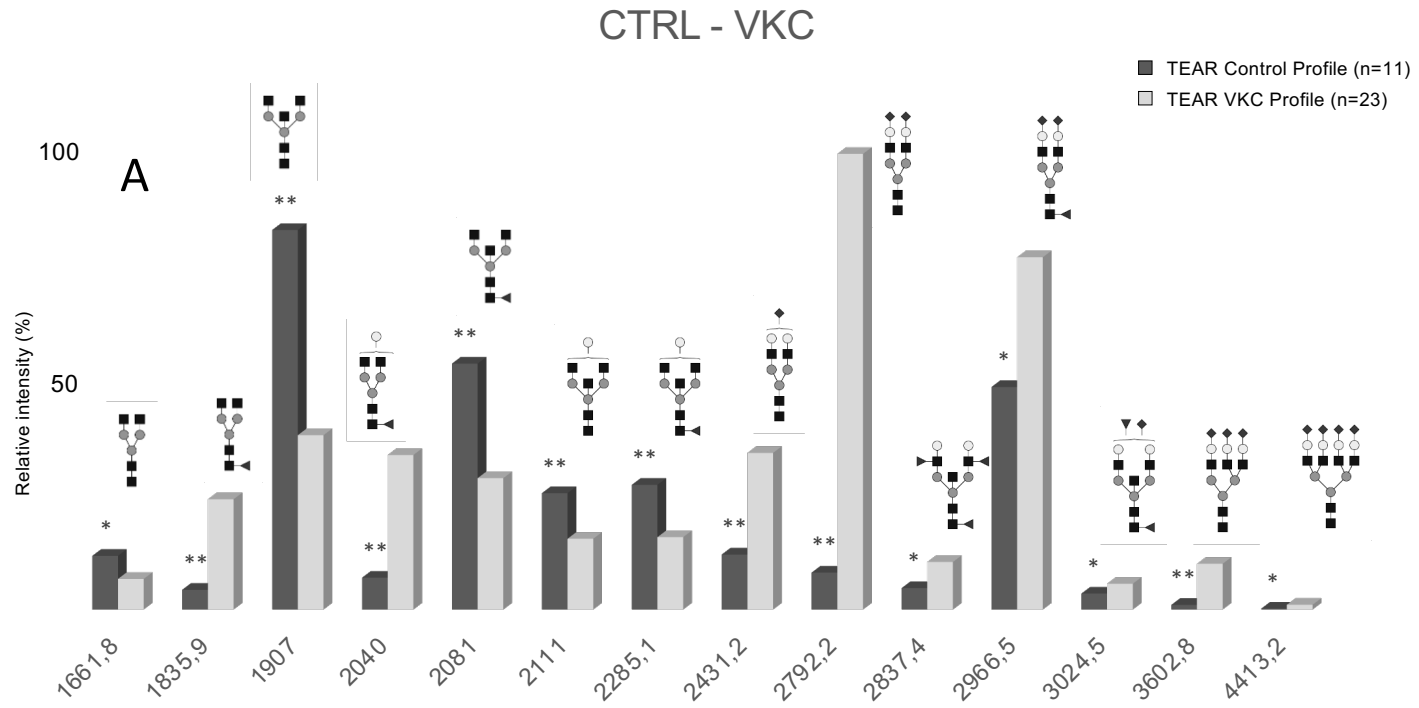
CTRL - VKC
TEAR Control Profile (n=11)
TEAR VKC Profile (n=23)
A
100
50
Relative intensity (%)
1661,8
1835,9
1907
2040
2081
2111
2285,1
2431,2
2792,2
2837,4
2966,5
3024,5
3602,8
4413,2

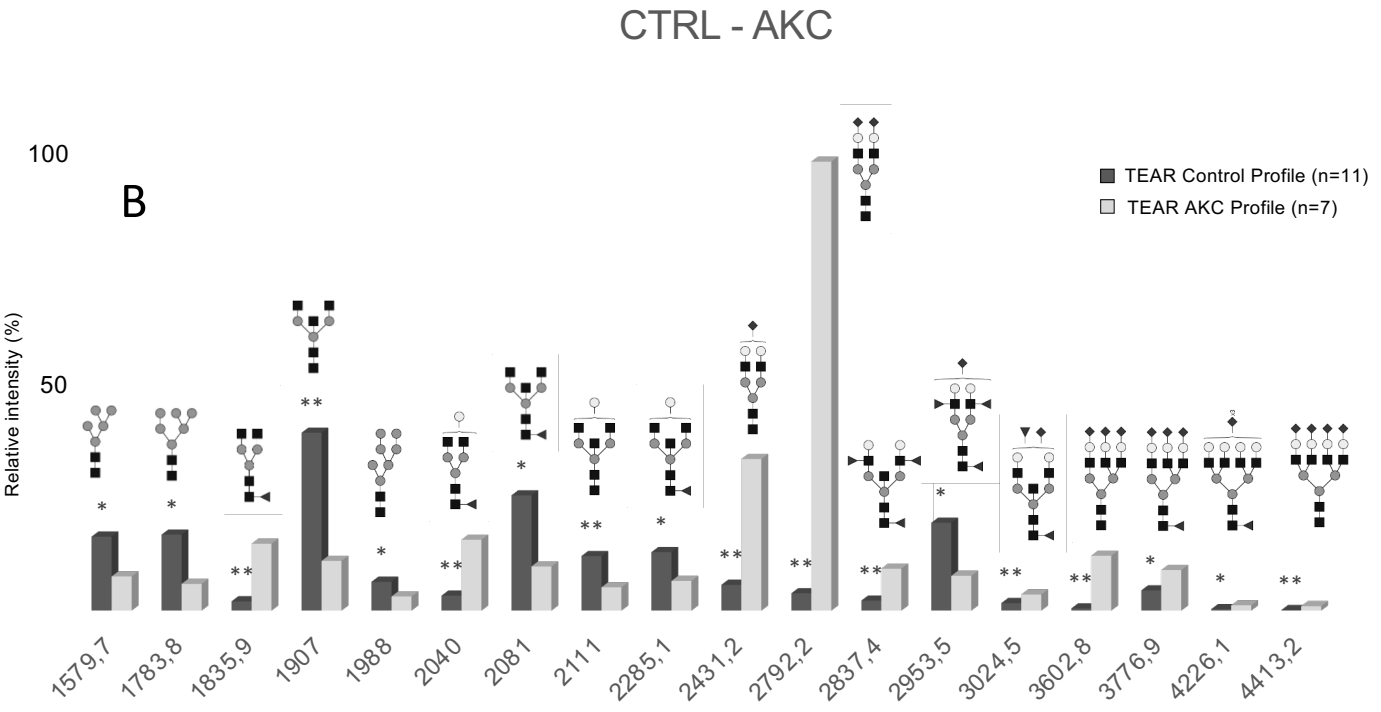
CTRL - AKC
TEAR Control Profile (n=11)
TEAR AKC Profile (n=7)
B
100
50
Relative intensity (%)
1579,7
1783,8
1835,9
1907
1988
2040
2081
2111
2285,1
2431,2
2792,2
2837,4
2953,5
3024,5
3602,8
3776,9
4226,1
4413,2

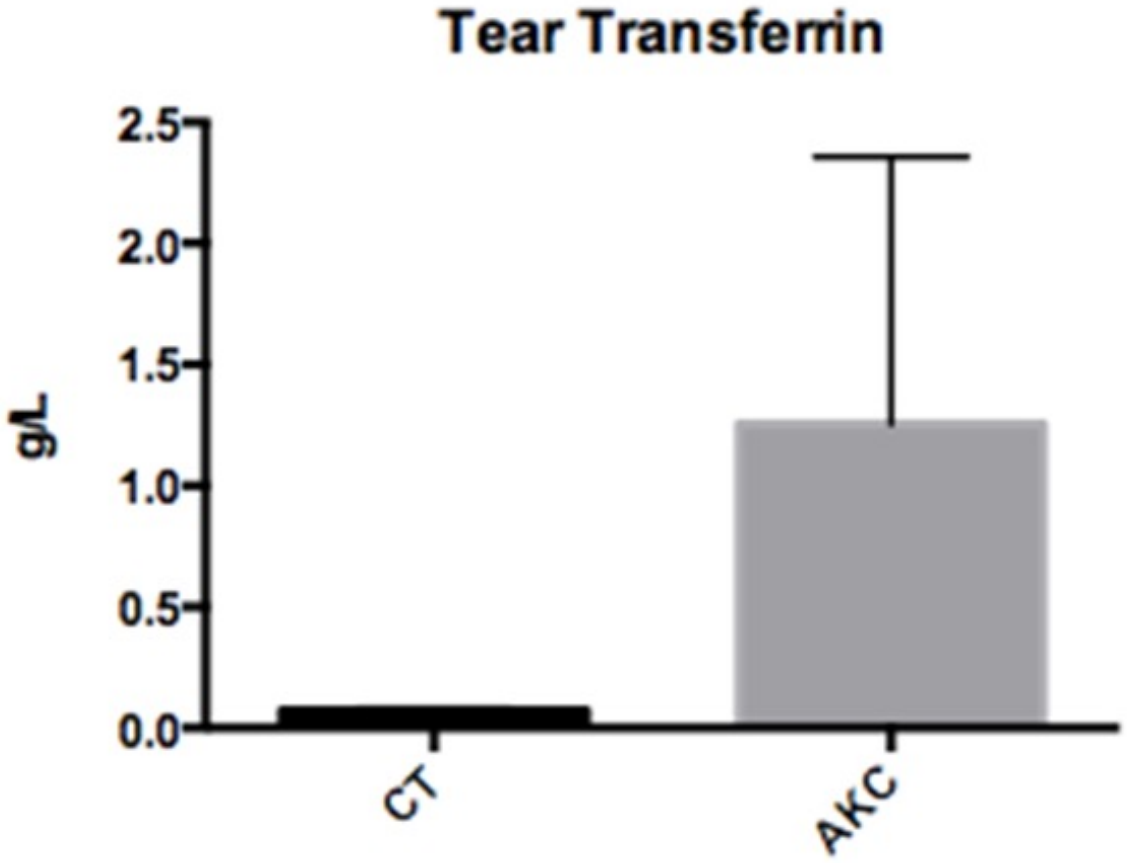
Tear Transferrin
2.5
2.0
1.5
1.0
0.5
0.0
g/L
CT
AKC

Supplementary Materials

Supplementary Table 1. Clinical data from VKC and AKC patients

Supplementary Table 2. Instrument parameters employed for MS analyses

Supplementary Table 3. Instrument parameters employed for MS/MS analyses

Supplementary Table 4. *N*-glycans identified in human tears

Supplementary Table 5. Structures of Lewis determinants

Table S1. Clinical data from VKC and AKC patients.

Patient	Gender	Age	Clinical form	Disease's activity score (0-4)
VKC-1	M	40	Mixed	2
VKC-2	F	17	Tarsal	4
VKC-3	M	6	Tarsal	3
VKC-4	M	7	Tarsal	3
VKC-5	M	6	Mixed	3
VKC-6	M	18	Limbal	2
VKC-7	M	18	Limbal	2
VKC-8	M	14	Limbal	4
VKC-9	F	9	Limbal	1
VKC-10	M	10	Mixed	3
VKC-11	M	9	Tarsal	3
VKC-12	M	7	Tarsal	3
VKC-13	M	13	Tarsal	4
VKC-14	M	9	Mixed	4
VKC-15	F	6	Limbal	2
VKC-16	M	7	Limbal	1
VKC-17	M	40	Limbal	2
VKC-18	F	28	Tarsal	2
VKC-19	F	13	Tarsal	4
VKC-20	M	5	Tarsal	4
VKC-21	F	27	Limbal	2
VKC-22	M	8	Tarsal	4
VKC-23	M	29	Tarsal	2
AKC-1	M	16	Tarsal	4
AKC-2	M	19	Tarsal	3
AKC-3	F	8	Tarsal	2
AKC-4	F	20	Mixed	2
AKC-5	F	17	Tarsal	3
AKC-6	F	12	Mixed	3
AKC-7	M	20	Tarsal	2

Table S2. MS Instrument Parameters

Summary	
Serial Number	1108
Instrument Name	4800 Instrument
Calibration Coefficients	1.405267e+002 3.493302e-007 1.768484e-006
Spot	
Plate Name	tear_NGly_permIII_23set14
Plate Barcode	<<none>>
Spot Set Name	tear_NGly_permIII_23set14
Location X Min	39046.000
Location X Max	44473.000
Location Y Min	57926.000
Location Y Max	59302.000
Spectrum	
Rejected Sub-spectra	0
Mass Acc. Opt. Cal Types Updated	None
Rejected Shots	0
Update Default Calibration	Disabled
Stop Reason	Max number of subspectra acquired
Total Accumulations	60
Total Ion Count	2.402286e+007
Total Shots	6000
Job-Wide Interpretation	Disabled
Configured for LCMS Experiments	Disabled
Acquisition	
Method Name	MS Reflector Positive Sample_personal op mode
Mass Analysis Type	MS Reflector Positive Ion Mode
Laser Intensity Range	3602 To 3602
Processing	
Processing Method Name	Reflector default Calbration
Calibration Type	Default
Pressures	
Source 1	5.6e-007 torr
Source 2	2.7e-008 torr
TC Turbo	4.3e-002 torr

Table S3. MS/MS Instrument Parameters

Summary	
Processing Method Name	MSMS Default
Serial Number	1108
Calibration Type	Default
Instrument Name	4800
Calibration Coefficients	5.473545e+004 5.784595e-007 1.378430e-002 2.792520e+003
Spot	
Plate Name	tear_MSMS_21oct2014
Plate Barcode	<<none>>
Spot Set Name	tear_MSMS_21oct2014
Job Run Comments	<<none>>
Location X Min	43096.000
Location X Max	44285.000
Location Y Min	71440.000
Location Y Max	72502.000
Pressures	
Source 1	5.1e-007 torr
Source 2	2.4e-008 torr
TC Turbo	4.3e-002 torr
Spectrum	
Rejected Sub-spectra	0
Mass Acc. Opt. Cal Types Updated	None
Rejected Shots	0
Update Default Calibration	Disabled
Stop Reason	Max number of subspectra acquired
Total Accumulations	180
Total Shots	18000
Acquisition	
Method Name	MSMS 1kV Positive_personal op mode
Mass Analysis Type	MS-MS Positive Ion Mode
CID	Off
Metastable Suppressor	On
Precursor Mass Window Option	Relative
Precursor Mass Window Relative	560
Laser Intensity Range	4900 To 4900
Processing	
Processing method name	MSMS Default

Table S4. N-glycans identified in human tears

STRUCTURE	m/z	STRUCTURE	m/z	STRUCTURE	m/z	STRUCTURE	m/z
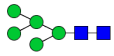	1579.8	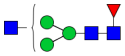	1590.8		1620.8	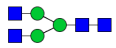	1661.8
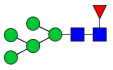	1753.9	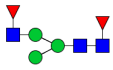	1764.9	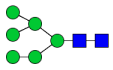	1783.9	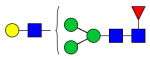	1794.9
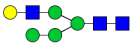	1824.9	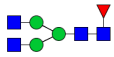	1835.9	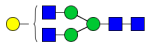	1865.9	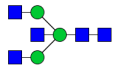	1907.0
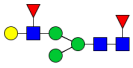	1969.0	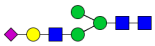	1982.0	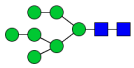	1988.0	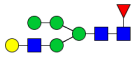	1999.0
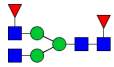	2010.0	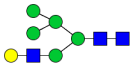	2029.0	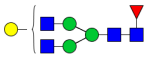	2040.0	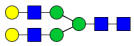	2070.0
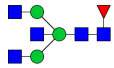	2081.1	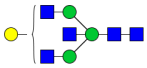	2111.1	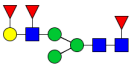	2143.1		2156.1
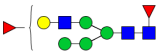	2173.1	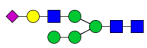	2186.1	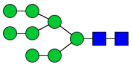	2192.1	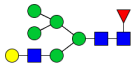	2203.1
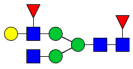	2214.1	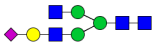	2227.1	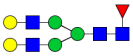	2244.1	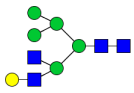	2274.1
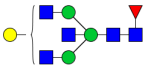	2285.2	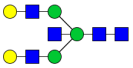	2315.2	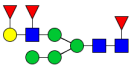	2347.2	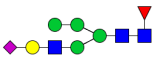	2360.2
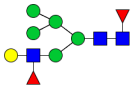	2377.2	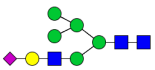	2390.2	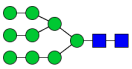	2396.2	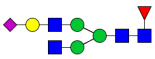	2401.2
	2418.2		2431.2		2448.2		2459.2
	2472.2		2489.3		2519.3		2564.3

STRUCTURE	m/z	STRUCTURE	m/z	STRUCTURE	m/z	STRUCTURE	m/z
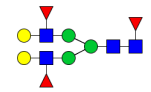	2592.3	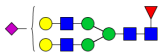	2605.3	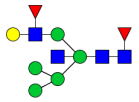	2622.3	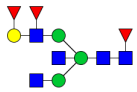	2633.3
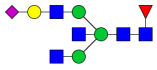	2646.3	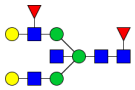	2663.3	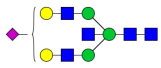	2676.3	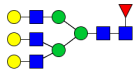	2693.4
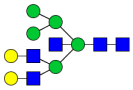	2723.4	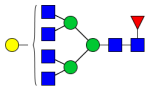	2734.4	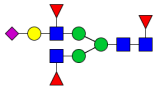	2749.4	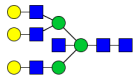	2764.4
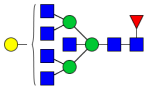	2775.4	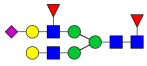	2779.4	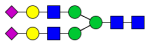	2792.4		2809.4
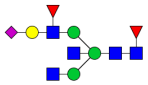	2820.4	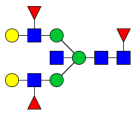	2837.4	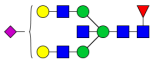	2850.4	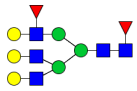	2867.4
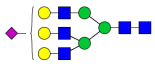	2880.4	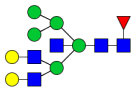	2897.5	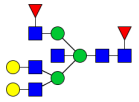	2908.5	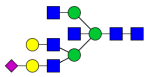	2921.5
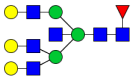	2938.5	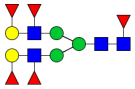	2940.5	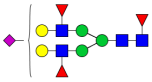	2953.5	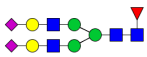	2966.5
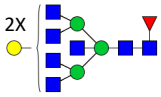	2979.5	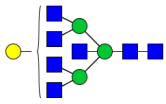	3009.5	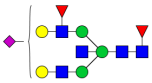	3024.5	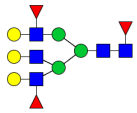	3041.5
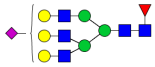	3054.5	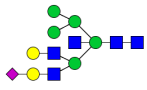	3084.5	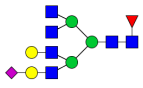	3095.6	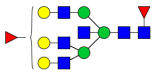	3112.6
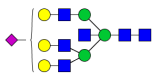	3125.6	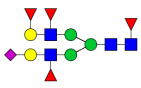	3127.6	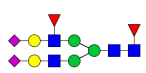	3140.6	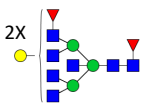	3153.6
	3185.6		3200.6		3215.6		3228.6

STRUCTURE	m/z	STRUCTURE	m/z	STRUCTURE	m/z	STRUCTURE	m/z
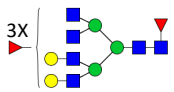	3256.6	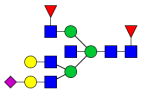	3269.6	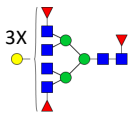	3286.7	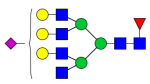	3299.7
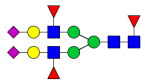	3314.7	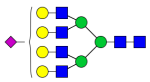	3329.7	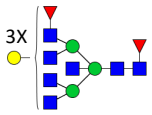	3357.7	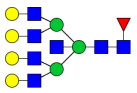	3387.7
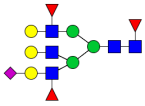	3402.7	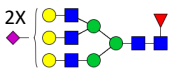	3415.7	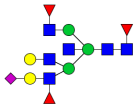	3443.7	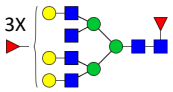	3460.7
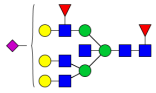	3473.7	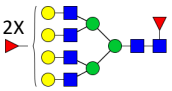	3490.8	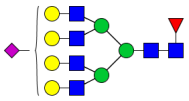	3503.8	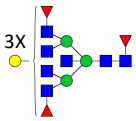	3531.8
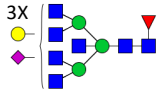	3544.8	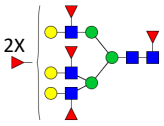	3563.8	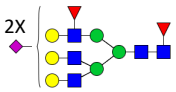	3589.8	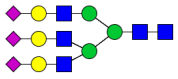	3602.8
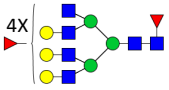	3634.8	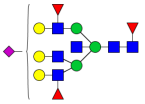	3647.8	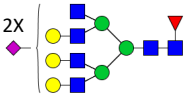	3660.8	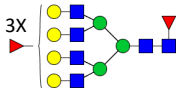	3664.8
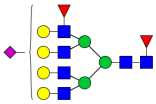	3677.8	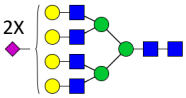	3690.8	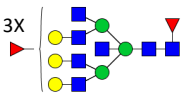	3705.9	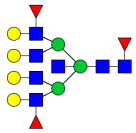	3735.9
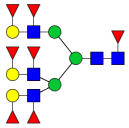	3737.9	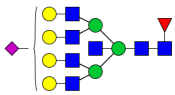	3748.9	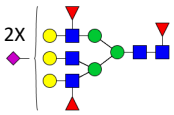	3763.9	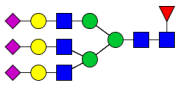	3776.9
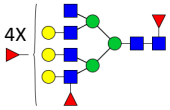	3808.9	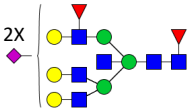	3834.9	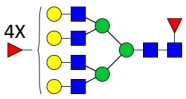	3838.9	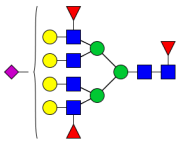	3851.9
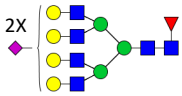	3864.9	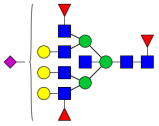	3893.0	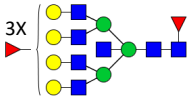	3910.0	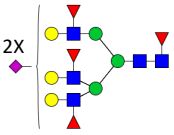	3938.0

STRUCTURE	m/z	STRUCTURE	m/z	STRUCTURE	m/z	STRUCTURE	m/z
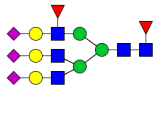	3951.0	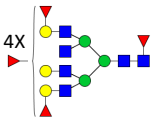	3983.0	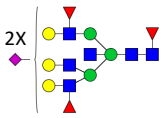	4009.0	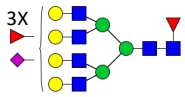	4026.0
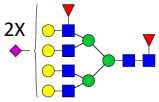	4039.0	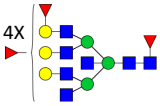	4054.0	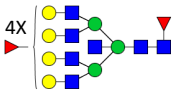	4084.1	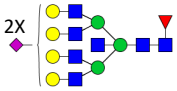	4110.1
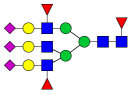	4125.1	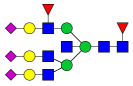	4196.1	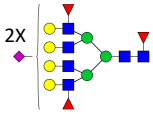	4213.1	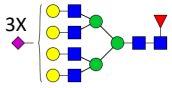	4226.1
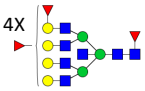	4258.1	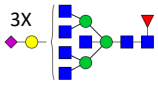	4267.1	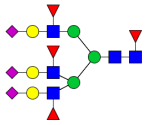	4299.1	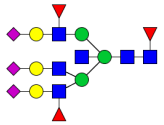	4370.2
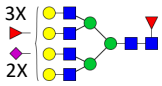	4387.2	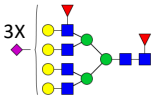	4400.2	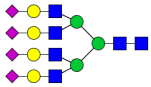	4413.2	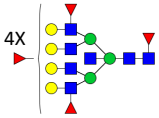	4432.2

Table S5. Structures of Lewis determinants.

Lewis a (Le^{a})	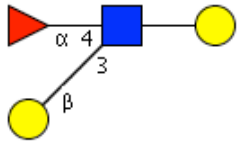
Lewis x (Le^{x})	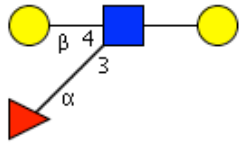
Lewis b (Le^{b})	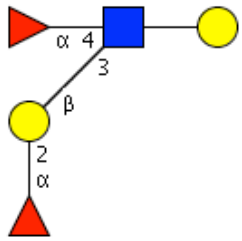
Lewis y (Le^{y})	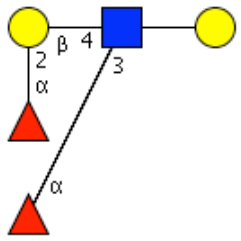
Sialyl- Lewis a (SLe^{a})	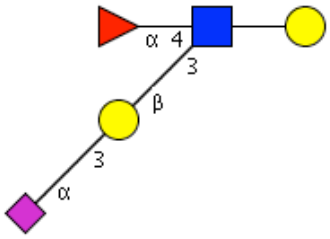
Sialyl- Lewis x (SLe^{x})	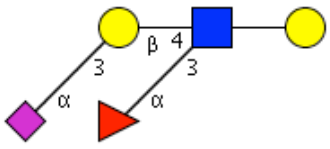

Supplementary Figure legends

Figures S1-S3: MALDI TOF mass spectra, with major assignments, of permethylated N-glycans released by PNGase F from control (CTRL) (S1), vernal keratoconjunctivitis (VKC) (S2) and atopic keratoconjunctivitis (AKC) (S3) tears.

Figures S4-S17: MALDI-TOF/TOF fragmentation analysis of the parent ion at *m/z* 1579.8, *m/z* 1783.9, *m/z* 1988.0, *m/z* 2192.1, *m/z* 2418.2, *m/z* 2592.3, *m/z* 2605.3, *m/z* 2766.4, *m/z* 3127.6, *m/z* 3140.6, *m/z* 3589.8, *m/z* 2940.5, *m/z* 2156.1, *m/z* 2360.2 respectively, present in the mass spectrum from a CTRL tear. MS/MS spectra recorded in several samples including VKC and AKC showed no differences.

N-acetylglucosamine (GlcNAc): blue square; Mannose (Man): green circle; Galactose (Gal): yellow circle; Sialic acid (NeuAc): purple lozenge; Fucose (Fuc): red triangle.

Figure S18: Comparison of statistically significant relative intensities between vernal keratoconjunctivitis (VKC) patients and atopic keratoconjunctivitis (AKC) patients. Only statistically significant glycans are shown.

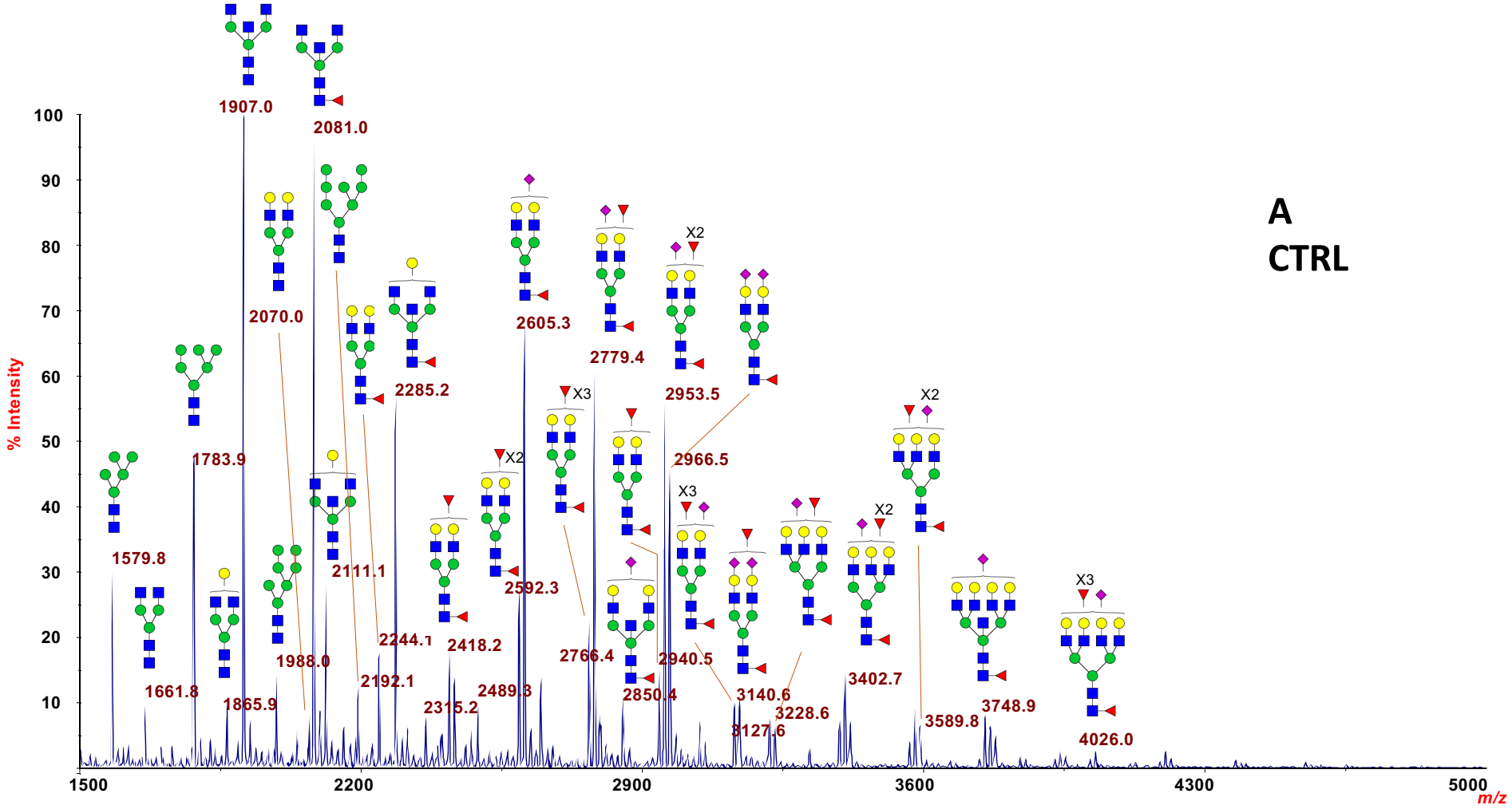
A
CTRL
% Intensity
m/z
100
90
80
70
60
50
40
30
20
10
1500
2200
2900
3600
4300
5000
1907.0
2081.0
2070.0
2605.3
2779.4
2953.5
2966.5
2285.2
1783.9
1579.8
2111.1
2592.3
2418.2
2244.1
1988.0
2192.1
1661.8
1865.9
2315.2
2489.3
2766.4
2850.4
2940.5
3140.6
3127.6
3228.6
3402.7
3589.8
3748.9
4026.0
X2
X3

S1

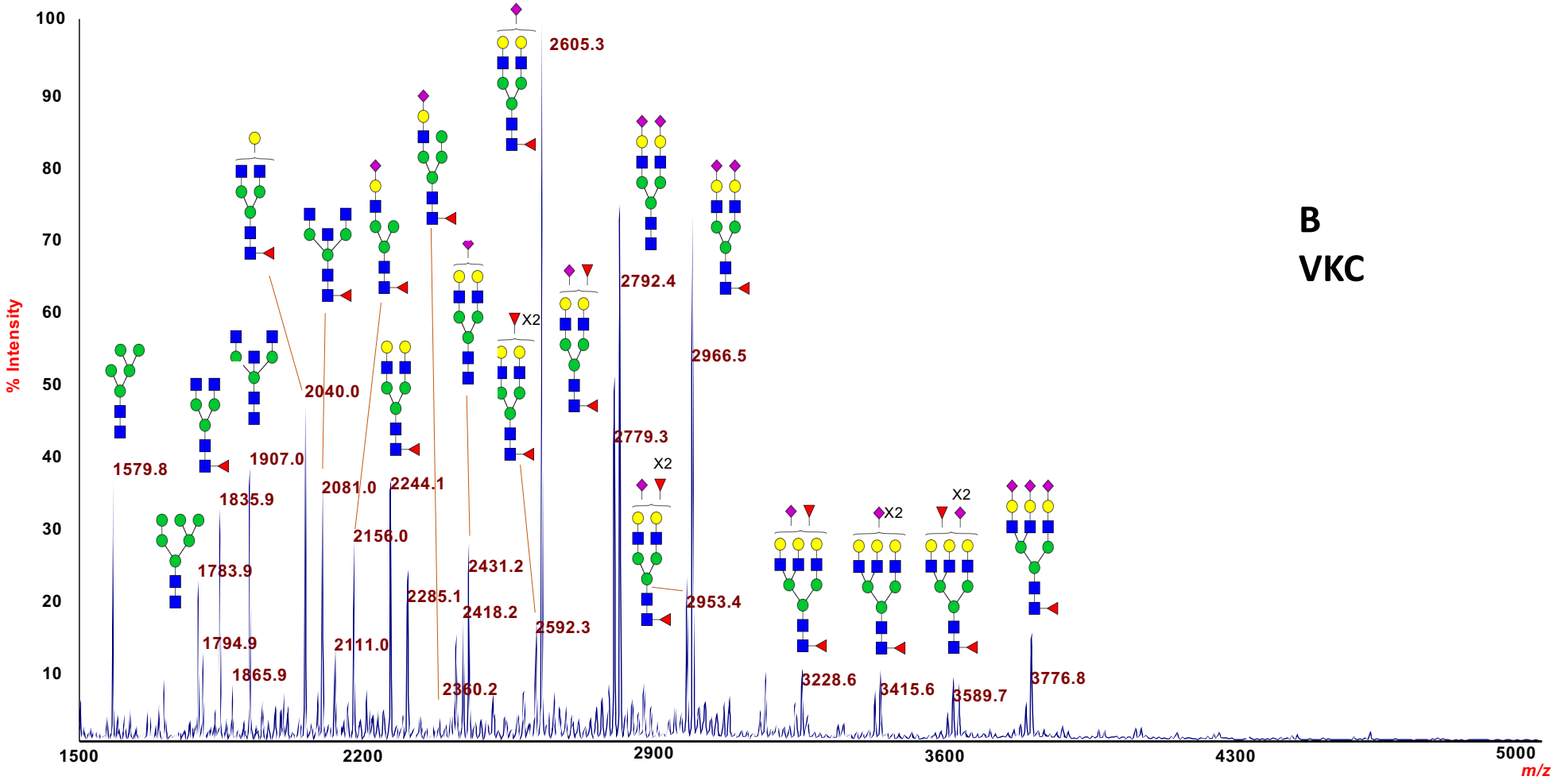
B
VKC
% Intensity
m/z
100
90
80
70
60
50
40
30
20
10
1500
2200
2900
3600
4300
5000
1579.8
1907.0
1835.9
2040.0
2081.0
2244.1
2156.0
1783.9
2431.2
2285.1
2418.2
1794.9
2111.0
1865.9
2592.3
2360.2
2605.3
2792.4
2966.5
2779.3
2953.4
3228.6
3415.6
3589.7
3776.8
X2

S2

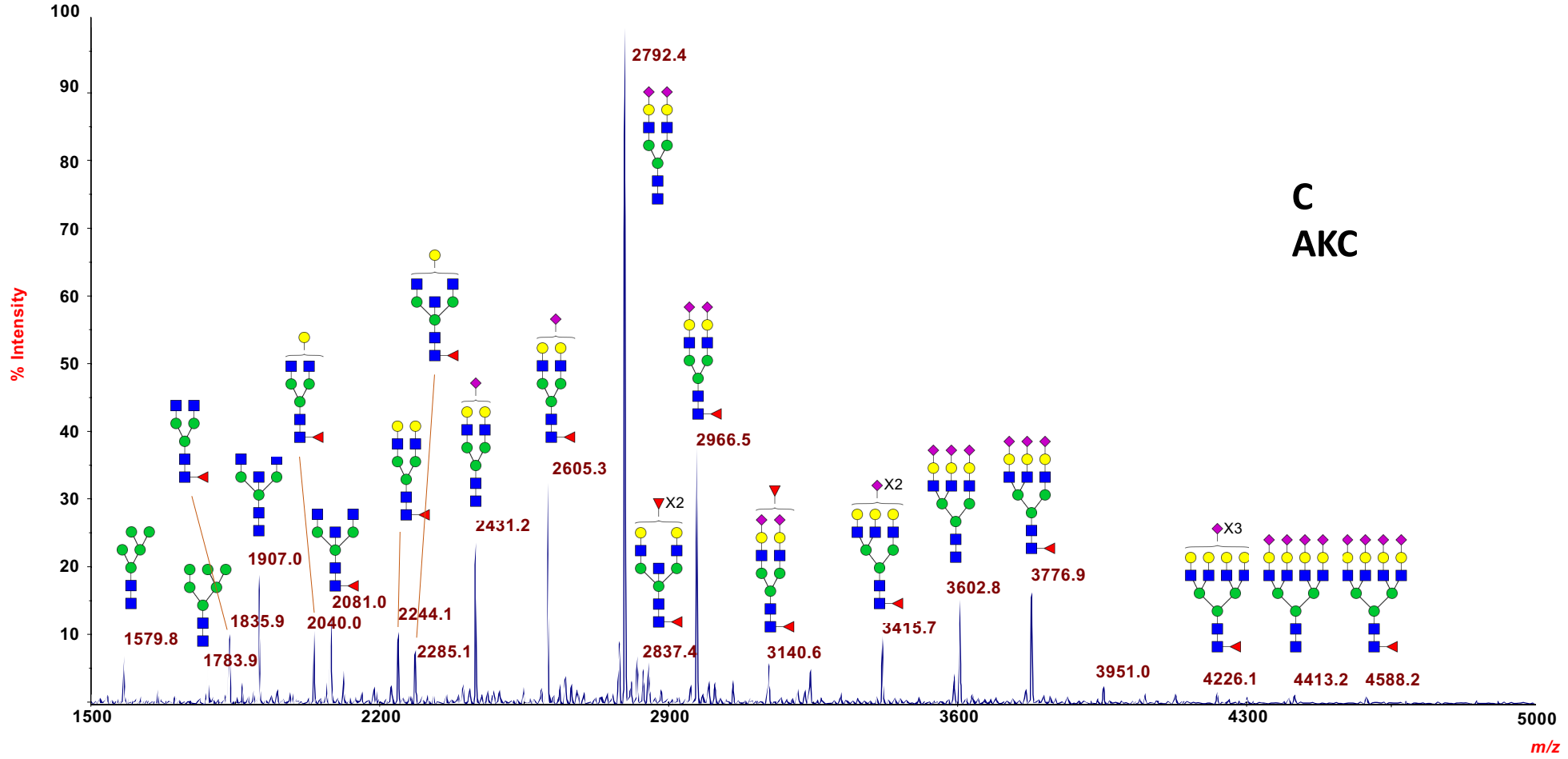
C
AKC
% Intensity
m/z
100
90
80
70
60
50
40
30
20
10
1500
2200
2900
3600
4300
5000
1579.8
1783.9
1835.9
1907.0
2040.0
2081.0
2244.1
2285.1
2431.2
2605.3
2792.4
2837.4
2966.5
3140.6
3415.7
3602.8
3776.9
3951.0
4226.1
4413.2
4588.2
X2
X2
X3

S3

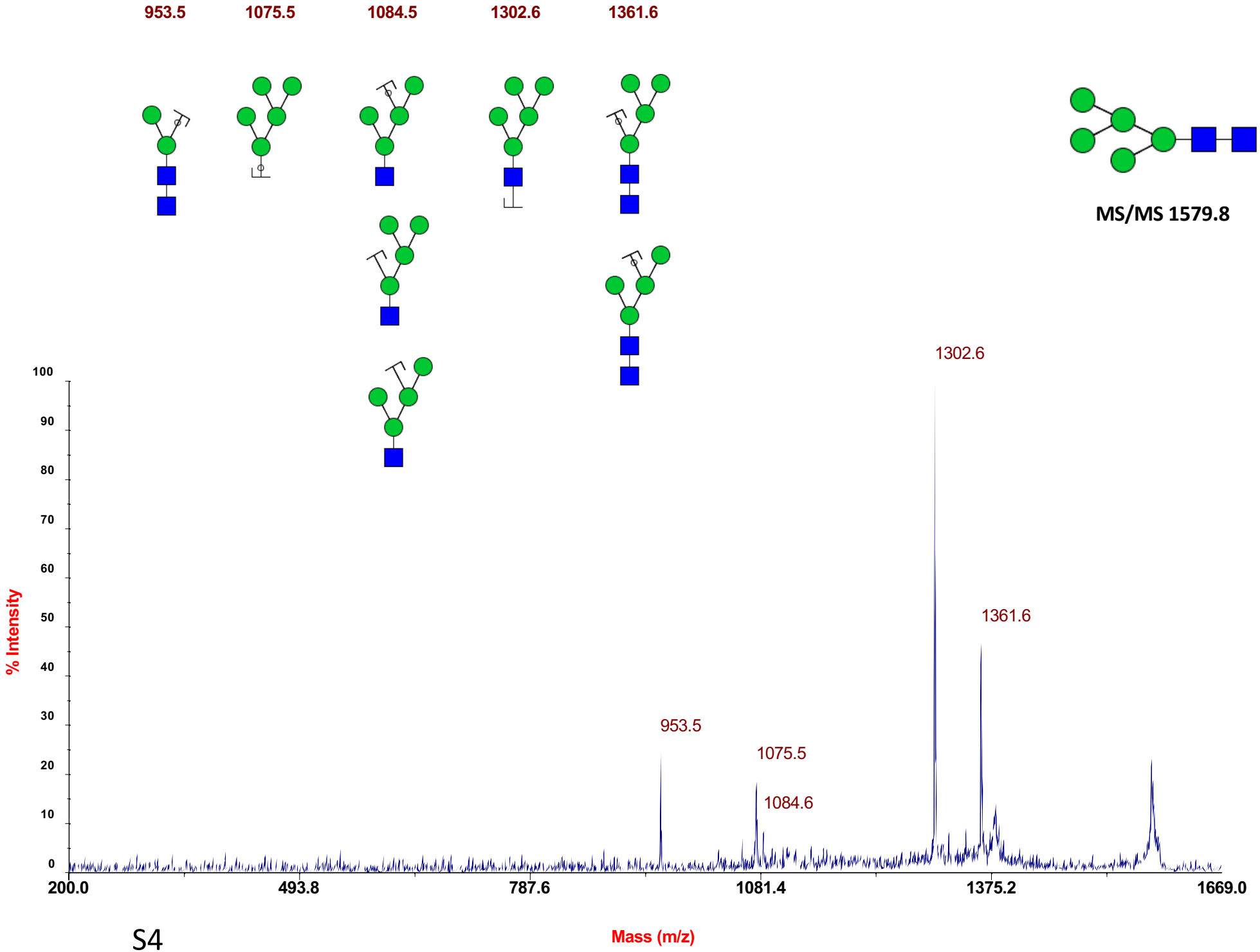
953.5
1075.5
1084.5
1302.6
1361.6
MS/MS 1579.8
% Intensity
100
90
80
70
60
50
40
30
20
10
0
1302.6
1361.6
953.5
1075.5
1084.6
200.0
493.8
787.6
1081.4
1375.2
1669.0
Mass (m/z)

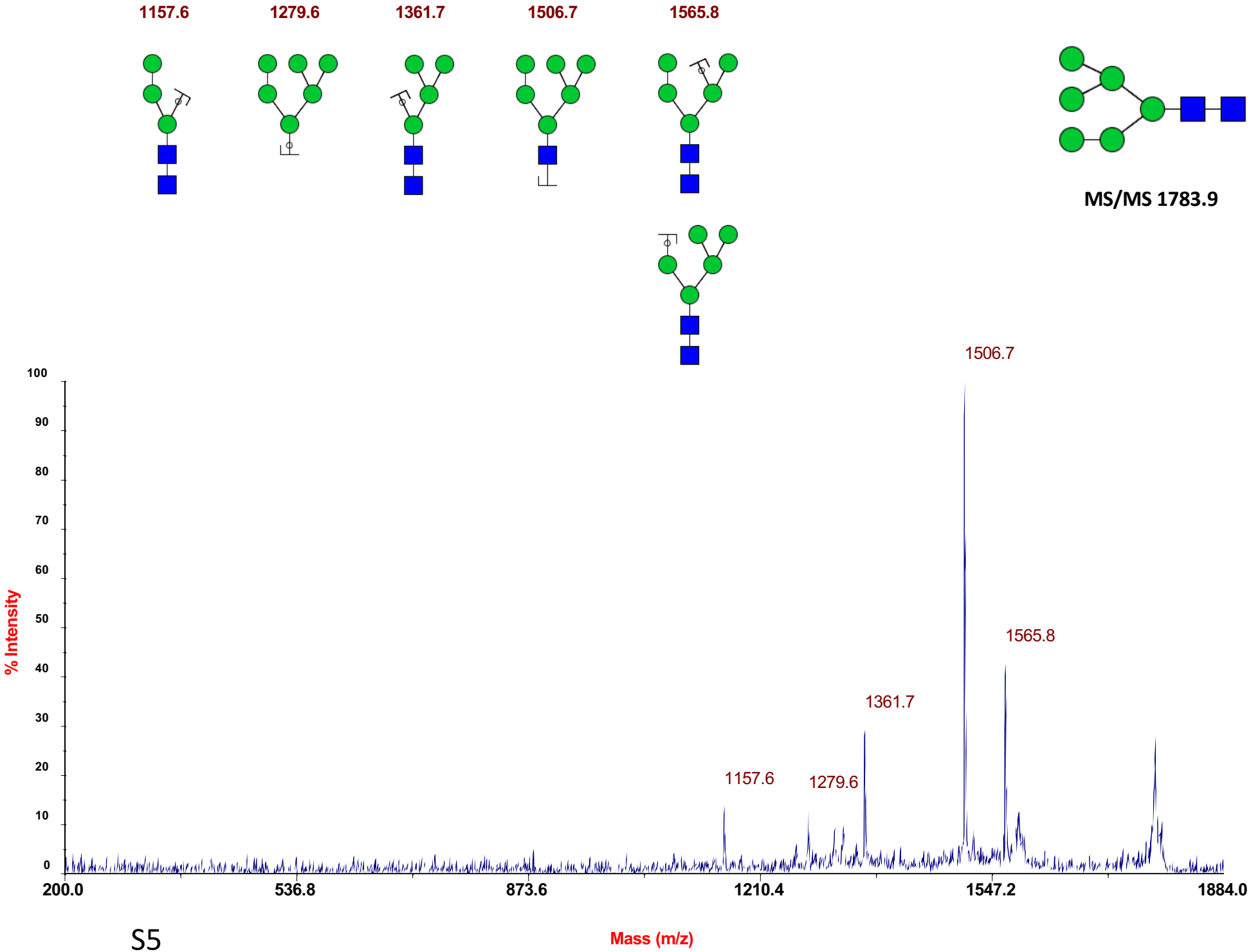
1157.6
1279.6
1361.7
1506.7
1565.8
MS/MS 1783.9
100
90
80
70
60
50
40
30
20
10
0
% Intensity
1506.7
1565.8
1361.7
1157.6
1279.6
200.0
536.8
873.6
1210.4
1547.2
1884.0
Mass (m/z)

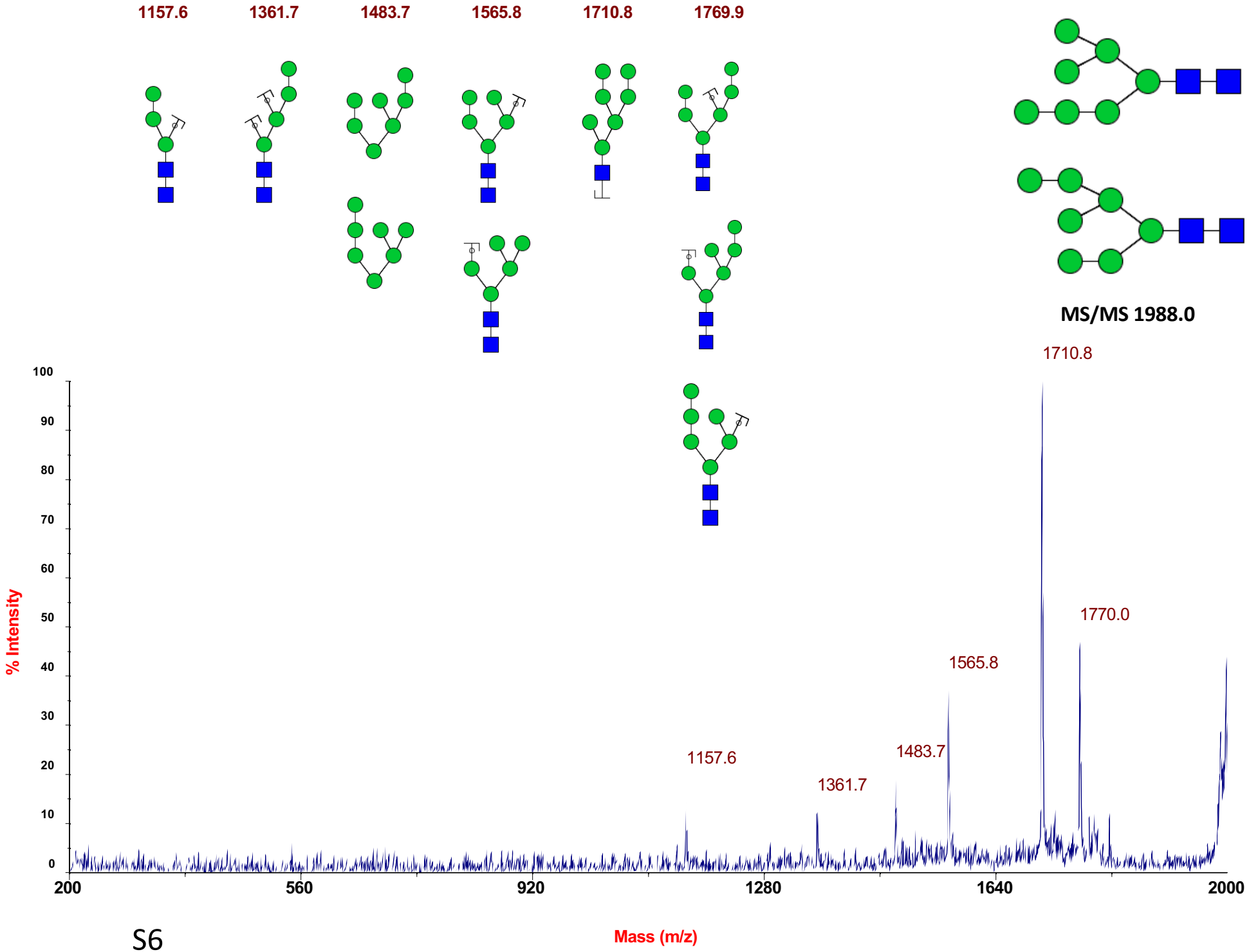
1157.6
1361.7
1483.7
1565.8
1710.8
1769.9
MS/MS 1988.0
1710.8
1770.0
1565.8
1483.7
1361.7
1157.6
% Intensity
Mass (m/z)
100
90
80
70
60
50
40
30
20
10
0
200
560
920
1280
1640
2000

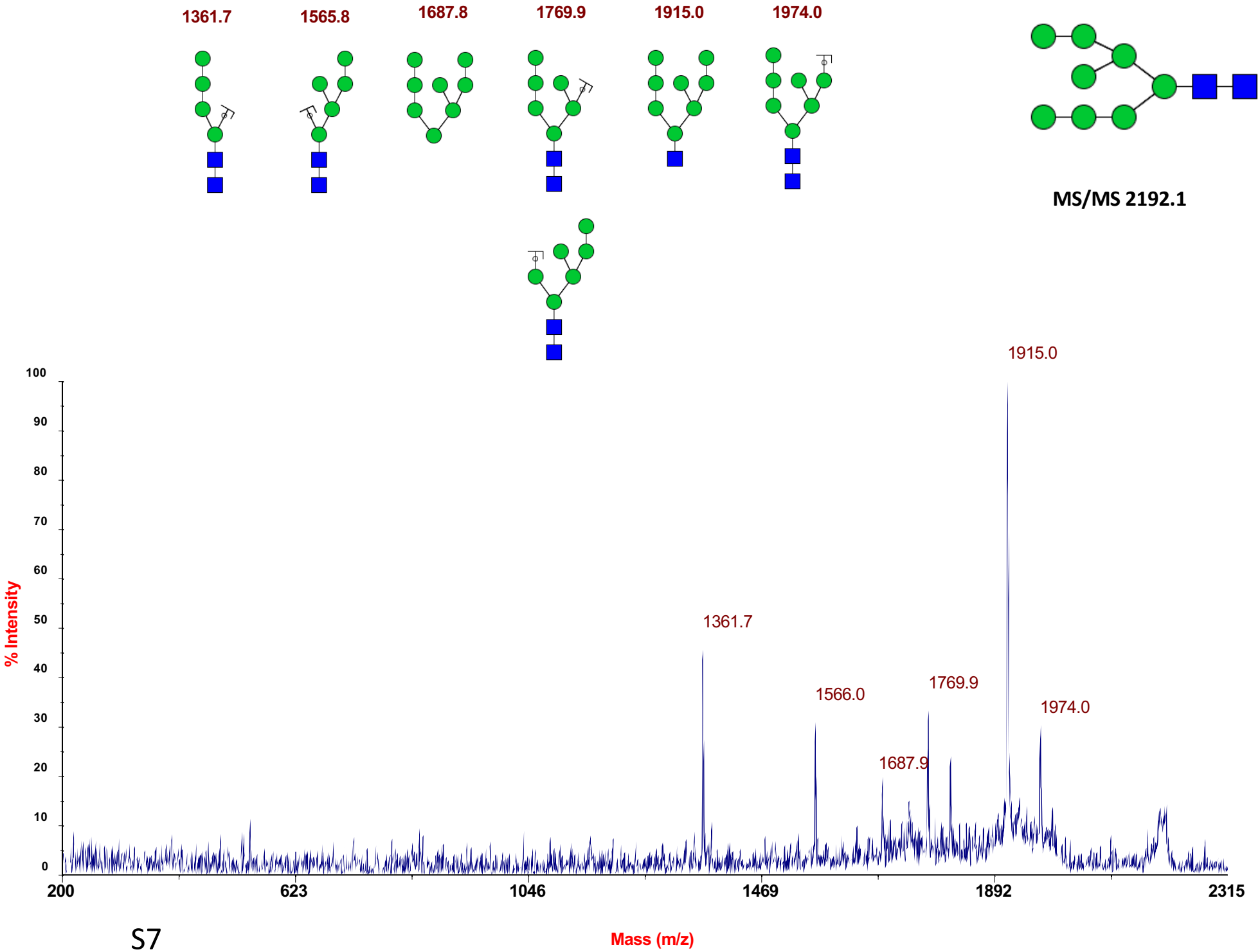
1361.7
1565.8
1687.8
1769.9
1915.0
1974.0
MS/MS 2192.1
% Intensity
100
90
80
70
60
50
40
30
20
10
0
1915.0
1361.7
1566.0
1769.9
1974.0
1687.9
200
623
1046
1469
1892
2315
Mass (m/z)

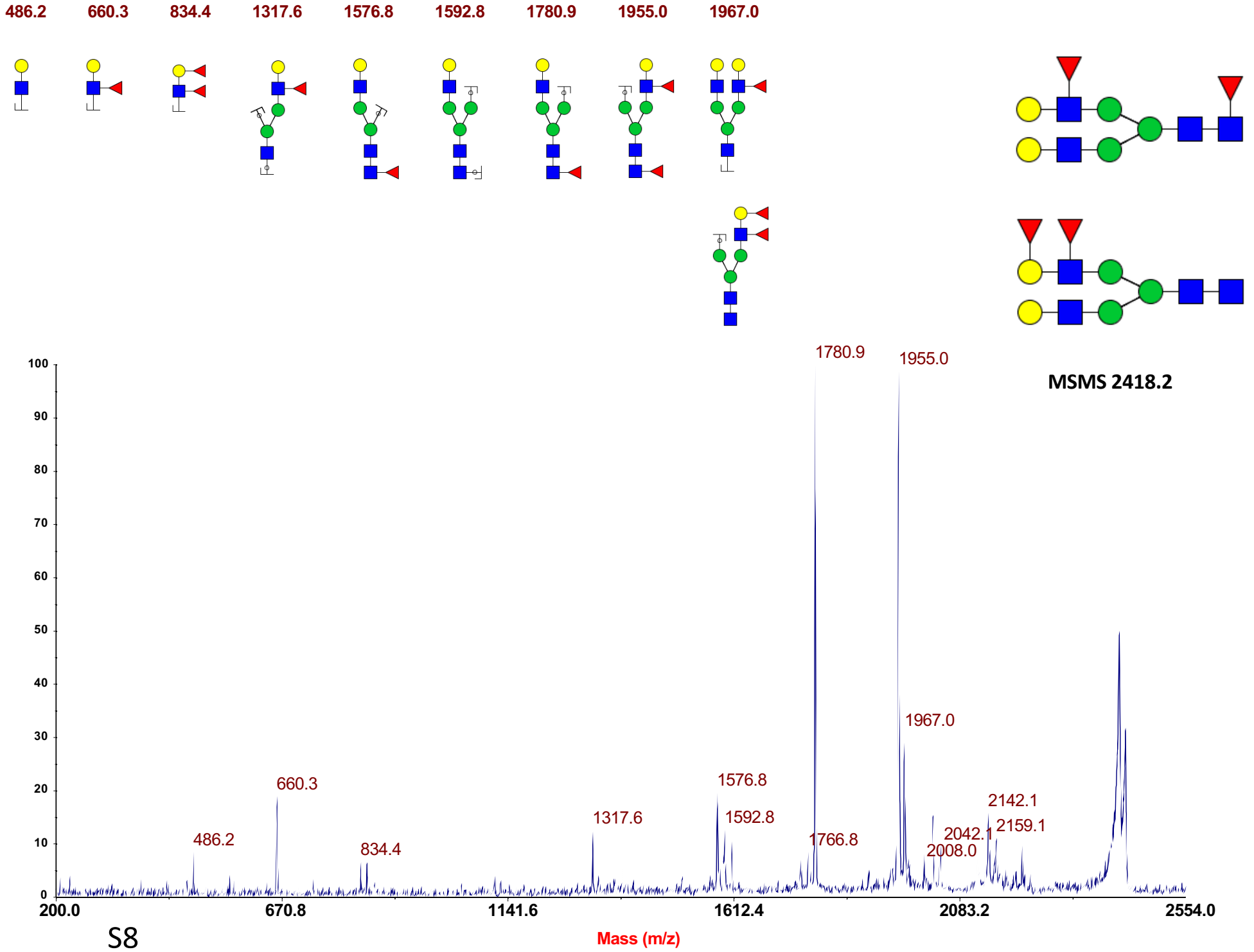
486.2
660.3
834.4
1317.6
1576.8
1592.8
1780.9
1955.0
1967.0
MSMS 2418.2
% Intensity
Mass (m/z)
100
90
80
70
60
50
40
30
20
10
0
200.0
670.8
1141.6
1612.4
2083.2
2554.0
1780.9
1955.0
1967.0
660.3
1576.8
1592.8
1317.6
2142.1
2159.1
2042.1
2008.0
1766.8
486.2
834.4

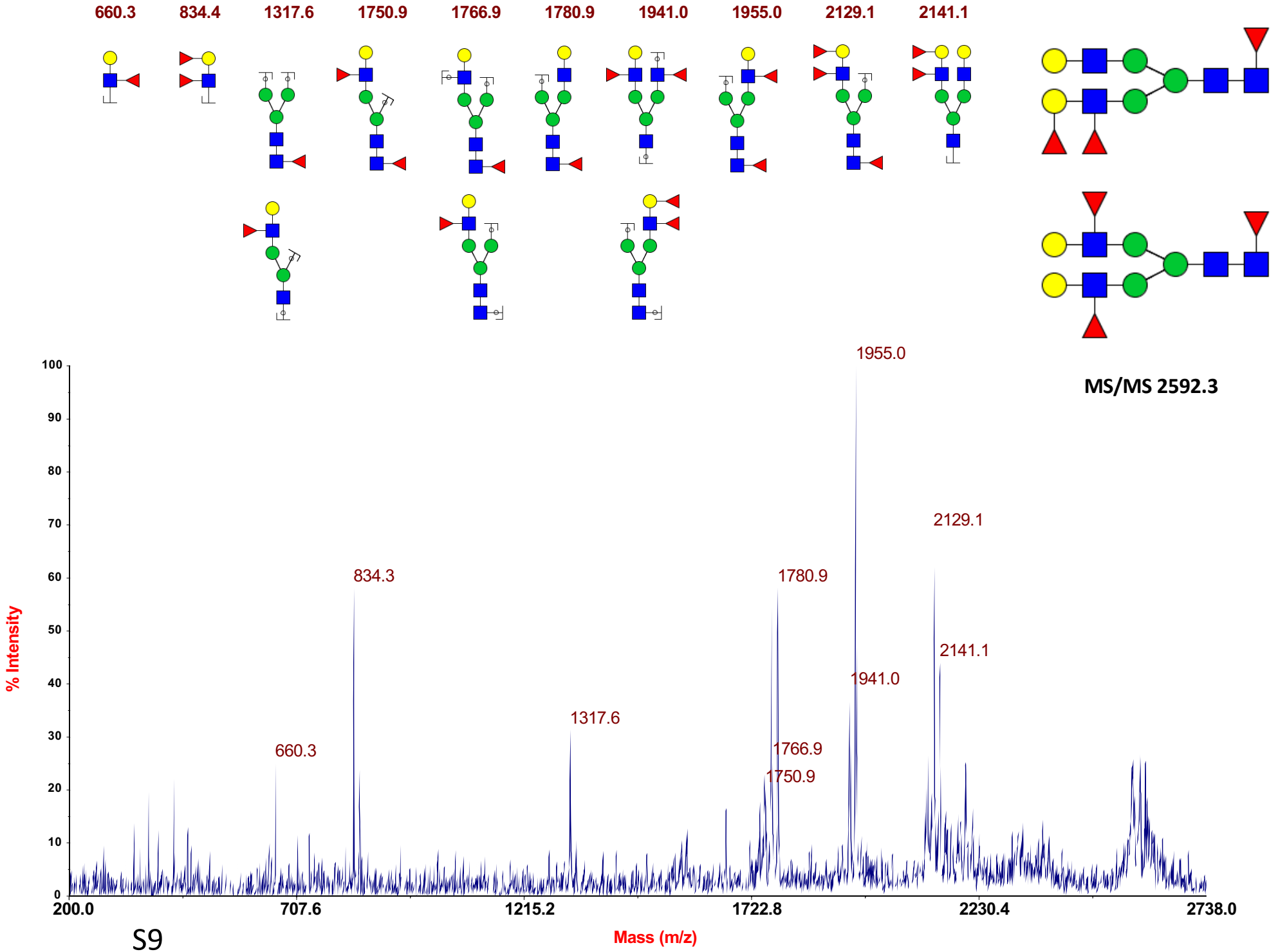
660.3
834.4
1317.6
1750.9
1766.9
1780.9
1941.0
1955.0
2129.1
2141.1
MS/MS 2592.3
% Intensity
Mass (m/z)
100
90
80
70
60
50
40
30
20
10
0
200.0
707.6
1215.2
1722.8
2230.4
2738.0

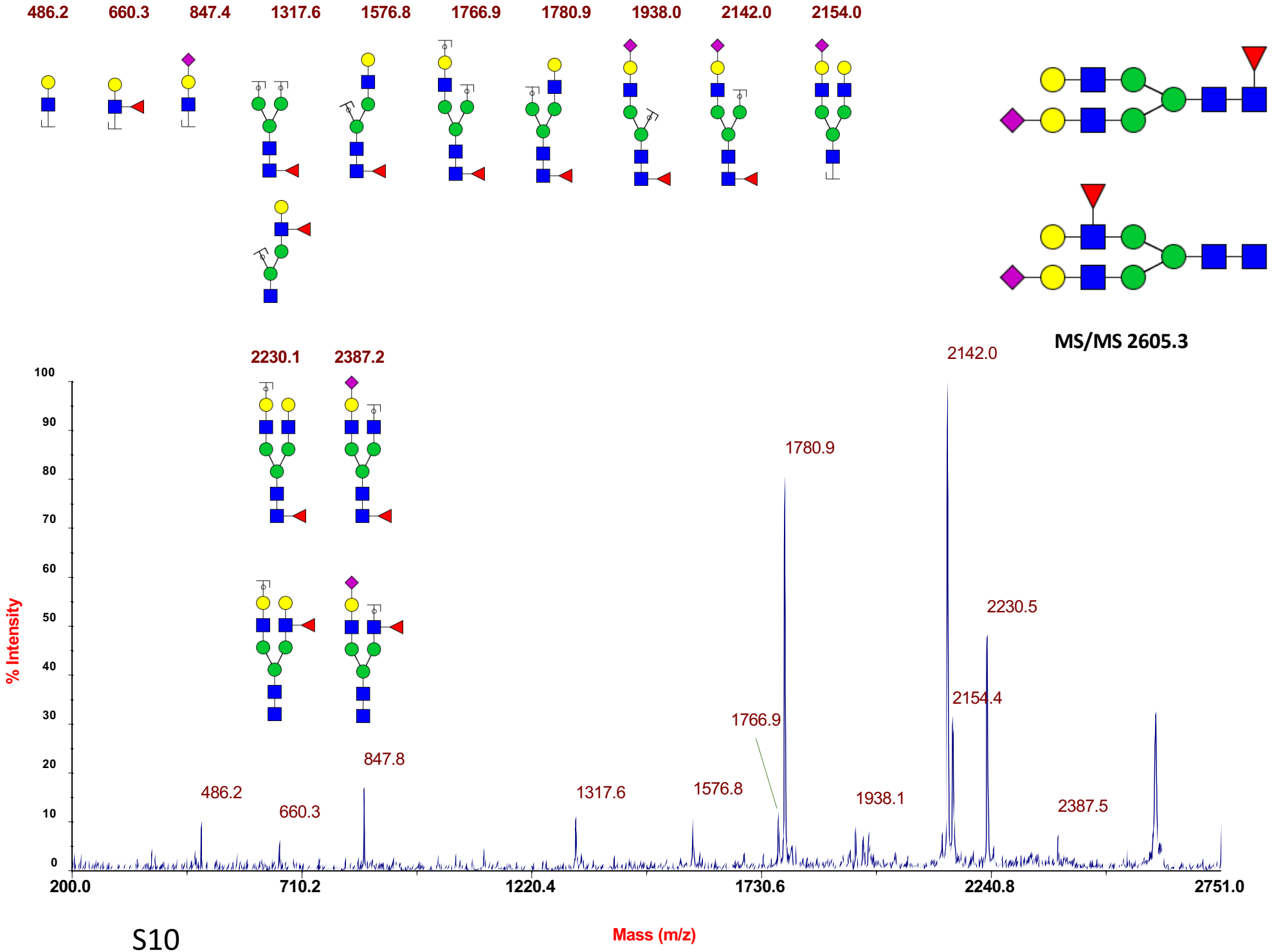
486.2
660.3
847.4
1317.6
1576.8
1766.9
1780.9
1938.0
2142.0
2154.0
2230.1
2387.2
MS/MS 2605.3
% Intensity
Mass (m/z)
100
90
80
70
60
50
40
30
20
10
0
200.0
710.2
1220.4
1730.6
2240.8
2751.0
2142.0
1780.9
2230.5
2154.4
1766.9
847.8
486.2
660.3
1317.6
1576.8
1938.1
2387.5

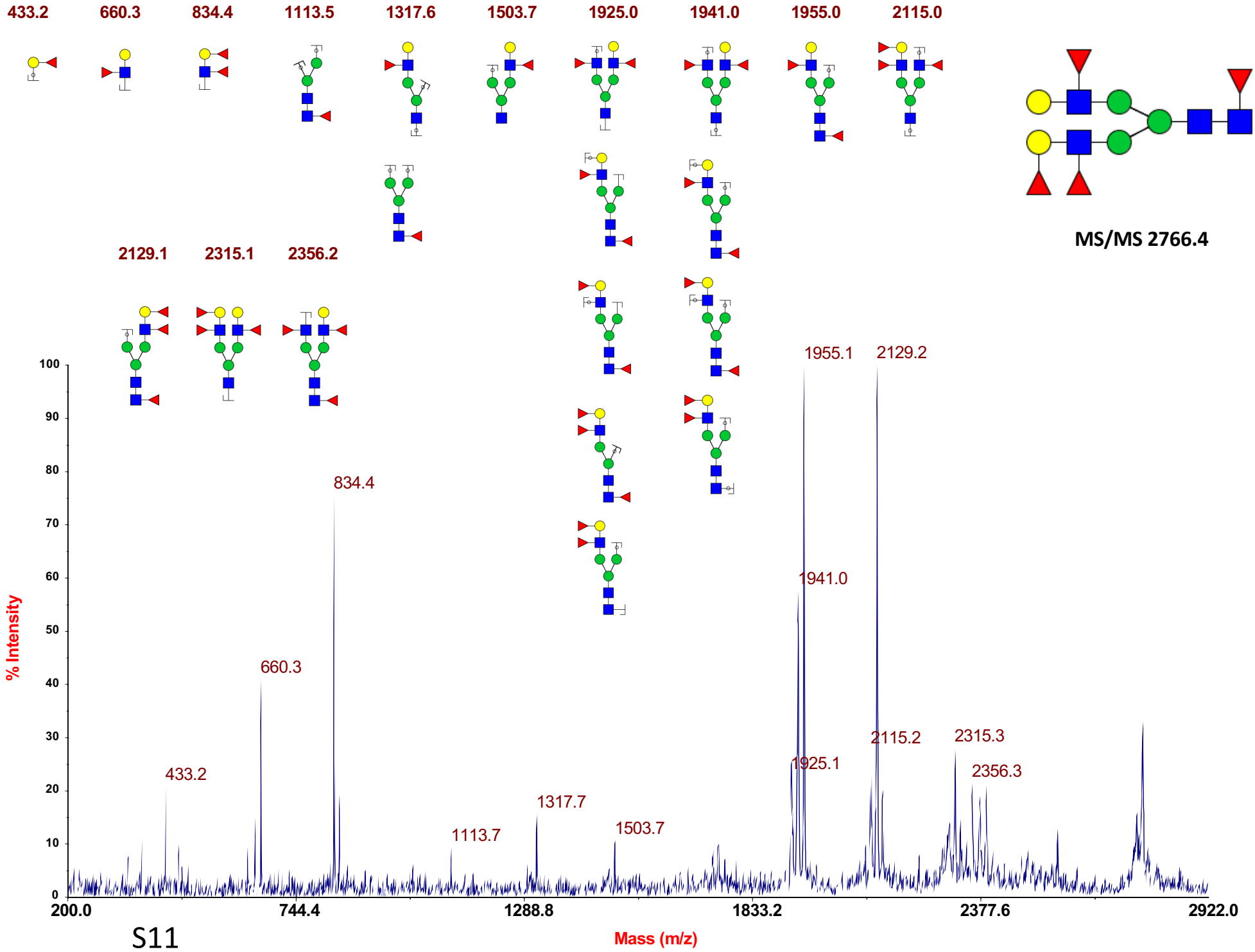
433.2
660.3
834.4
1113.5
1317.6
1503.7
1925.0
1941.0
1955.0
2115.0
2129.1
2315.1
2356.2
MS/MS 2766.4
% Intensity
Mass (m/z)
200.0
744.4
1288.8
1833.2
2377.6
2922.0
0
10
20
30
40
50
60
70
80
90
100
433.2
660.3
834.4
1113.7
1317.7
1503.7
1925.1
1941.0
1955.1
2115.2
2129.2
2315.3
2356.3

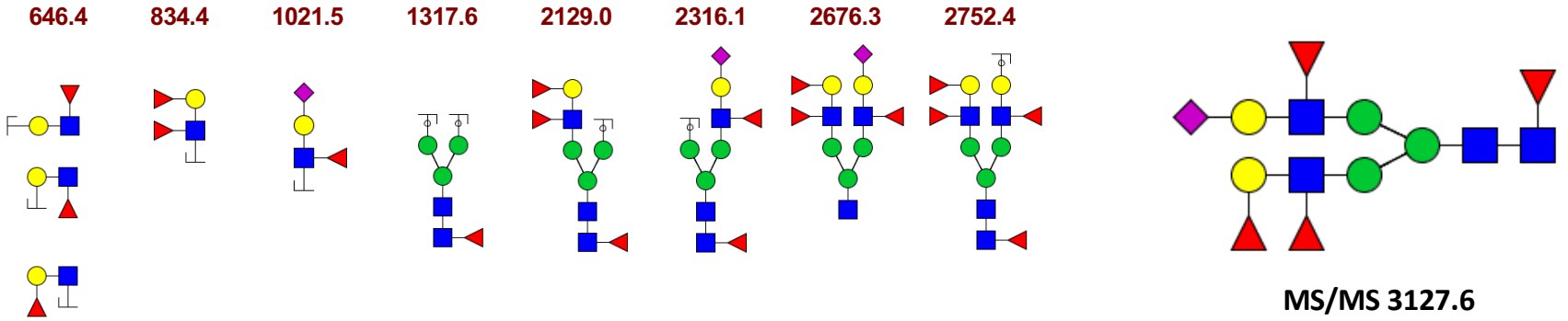
646.4
834.4
1021.5
1317.6
2129.0
2316.1
2676.3
2752.4
MS/MS 3127.6

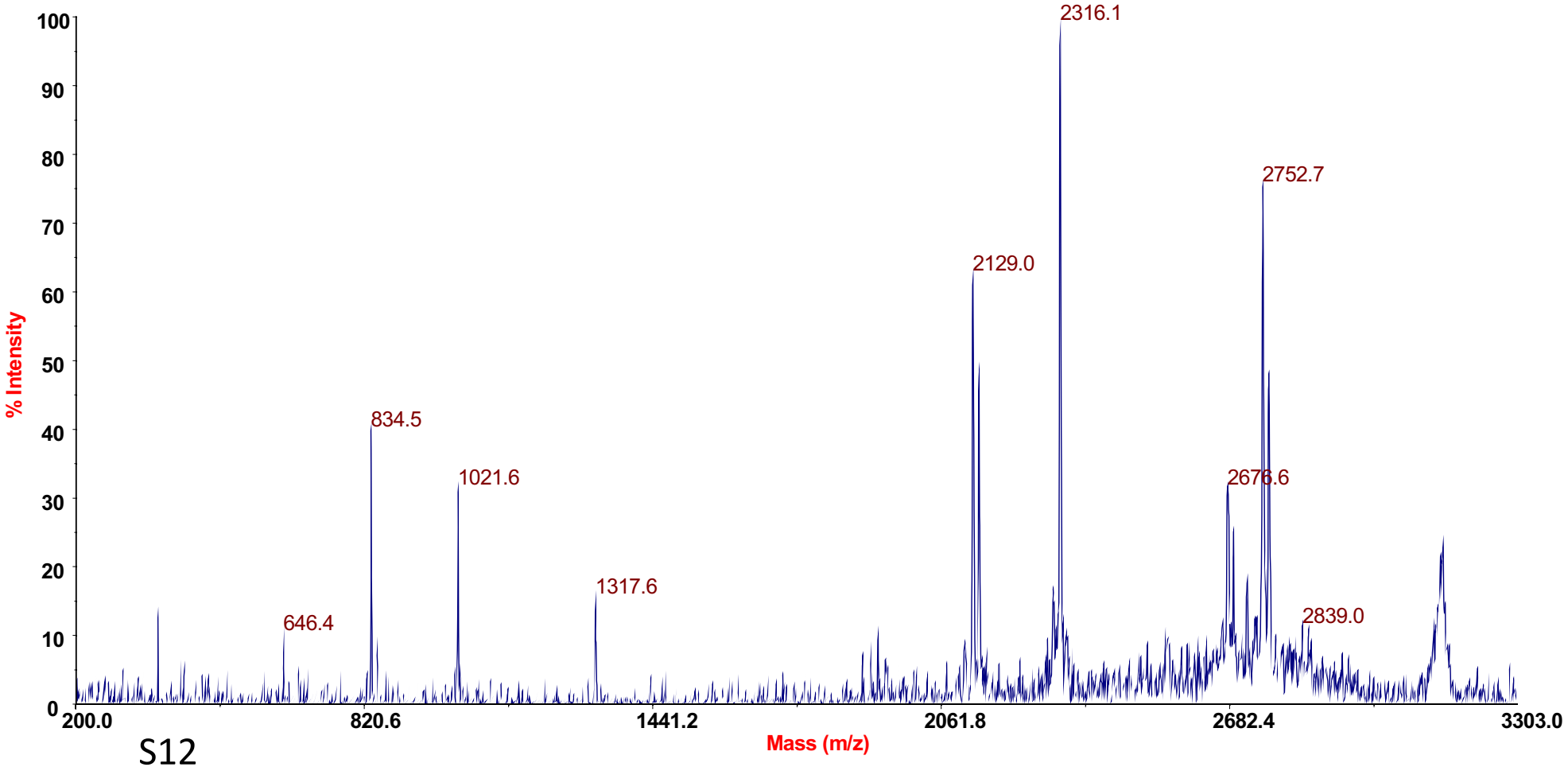
% Intensity
Mass (m/z)
100
90
80
70
60
50
40
30
20
10
0
200.0
820.6
1441.2
2061.8
2682.4
3303.0
2316.1
2752.7
2129.0
834.5
1021.6
2676.6
1317.6
646.4
2839.0

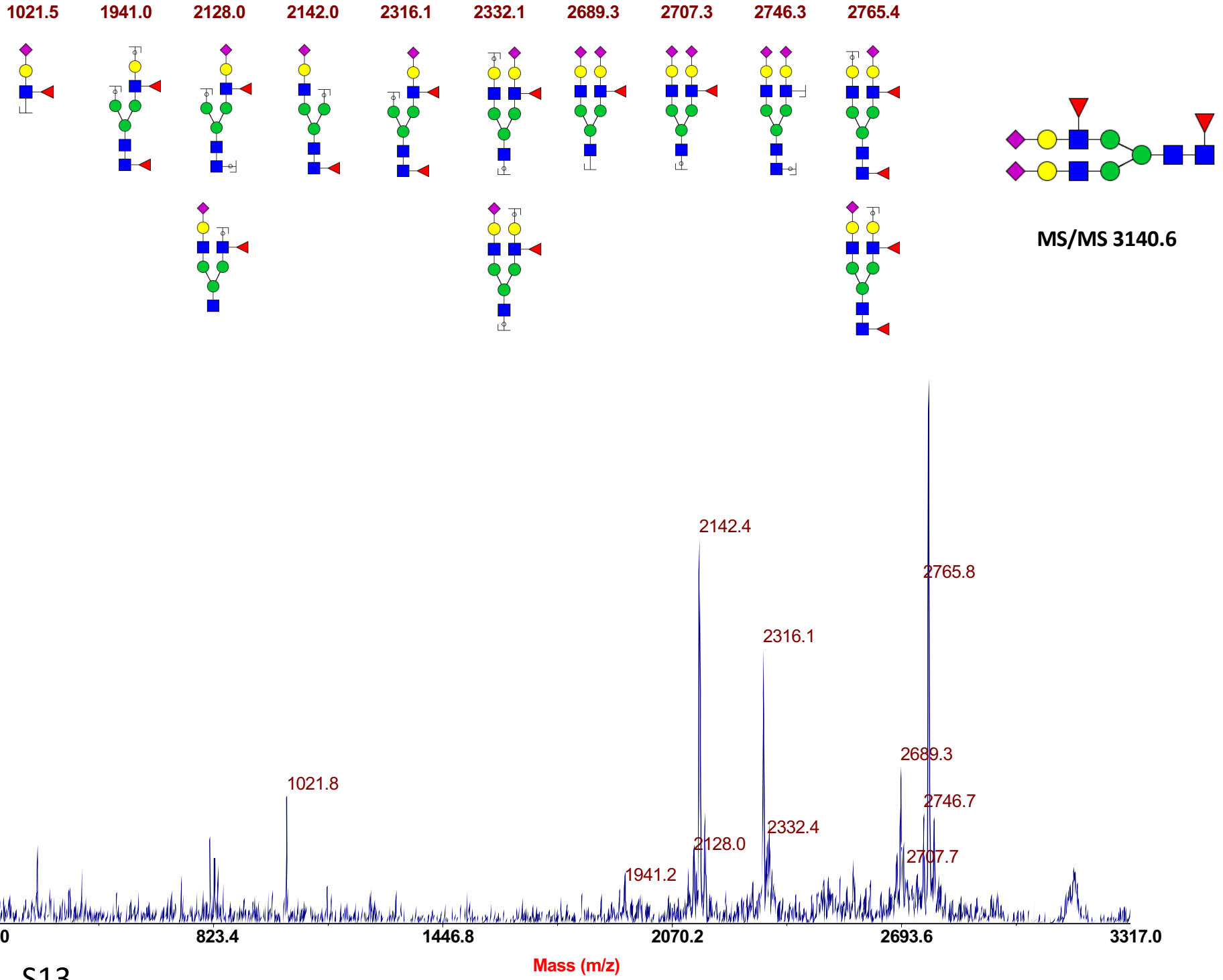
1021.5
1941.0
2128.0
2142.0
2316.1
2332.1
2689.3
2707.3
2746.3
2765.4
MS/MS 3140.6
% Intensity
Mass (m/z)
100
90
80
70
60
50
40
30
20
10
0
200.0
823.4
1446.8
2070.2
2693.6
3317.0
1021.8
1941.2
2128.0
2142.4
2316.1
2332.4
2689.3
2707.7
2746.7
2765.8

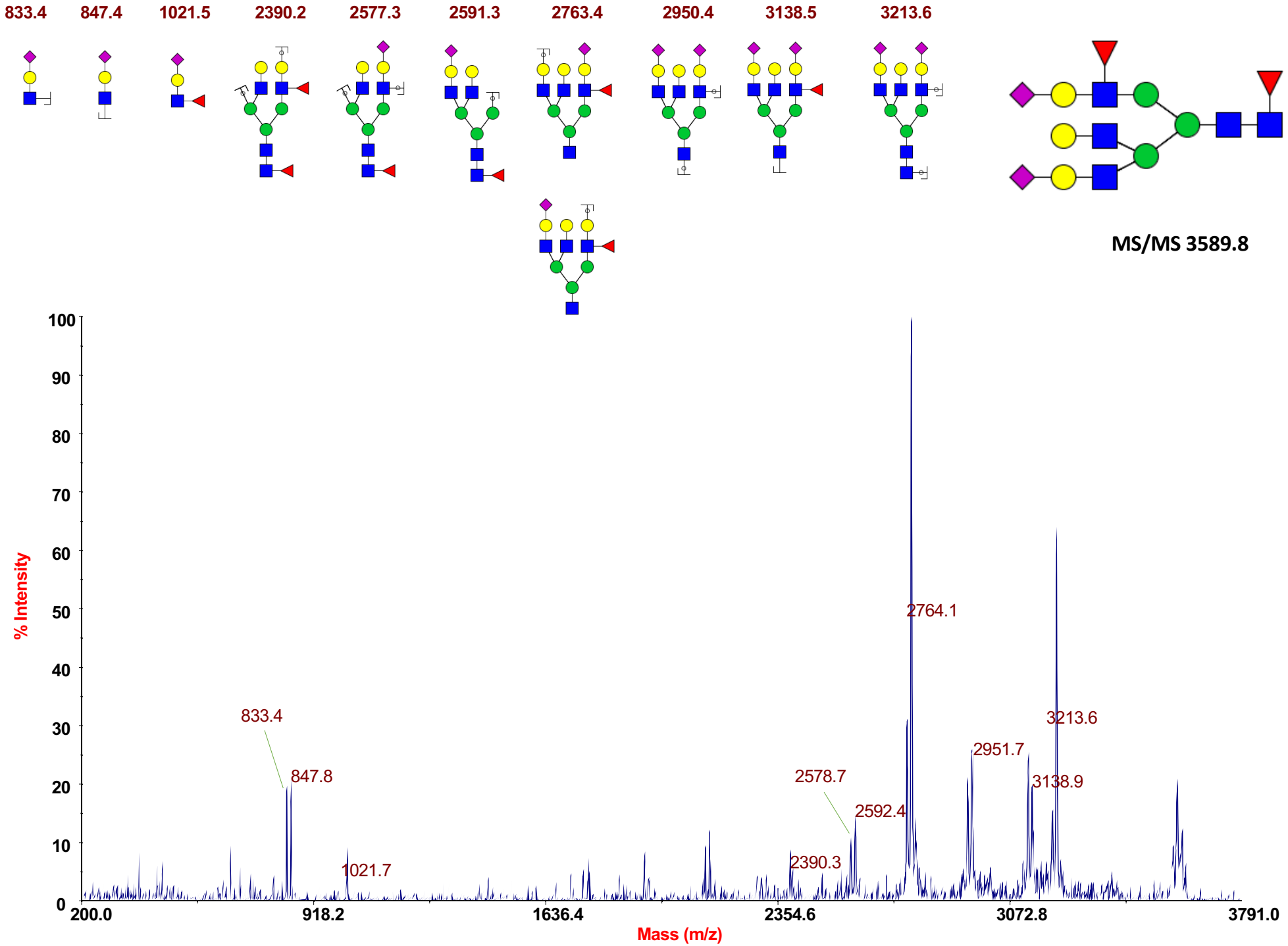
833.4
847.4
1021.5
2390.2
2577.3
2591.3
2763.4
2950.4
3138.5
3213.6
MS/MS 3589.8
% Intensity
Mass (m/z)
100
90
80
70
60
50
40
30
20
10
0
200.0
918.2
1636.4
2354.6
3072.8
3791.0
2764.1
833.4
847.8
1021.7
2578.7
2592.4
2390.3
2951.7
3138.9
3213.6

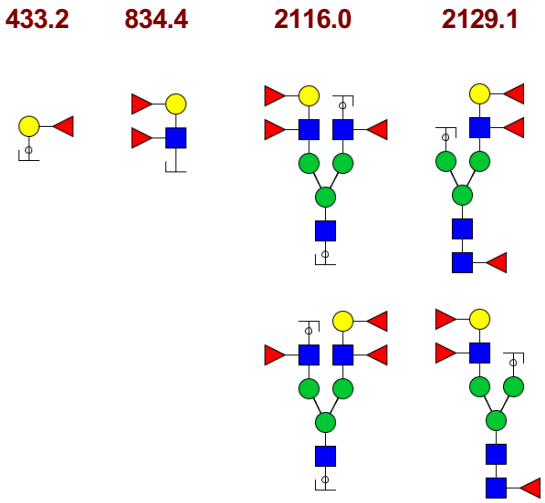
433.2
834.4
2116.0
2129.1

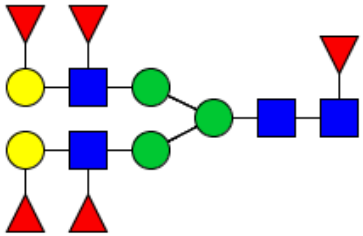

MS/MS 2940.5

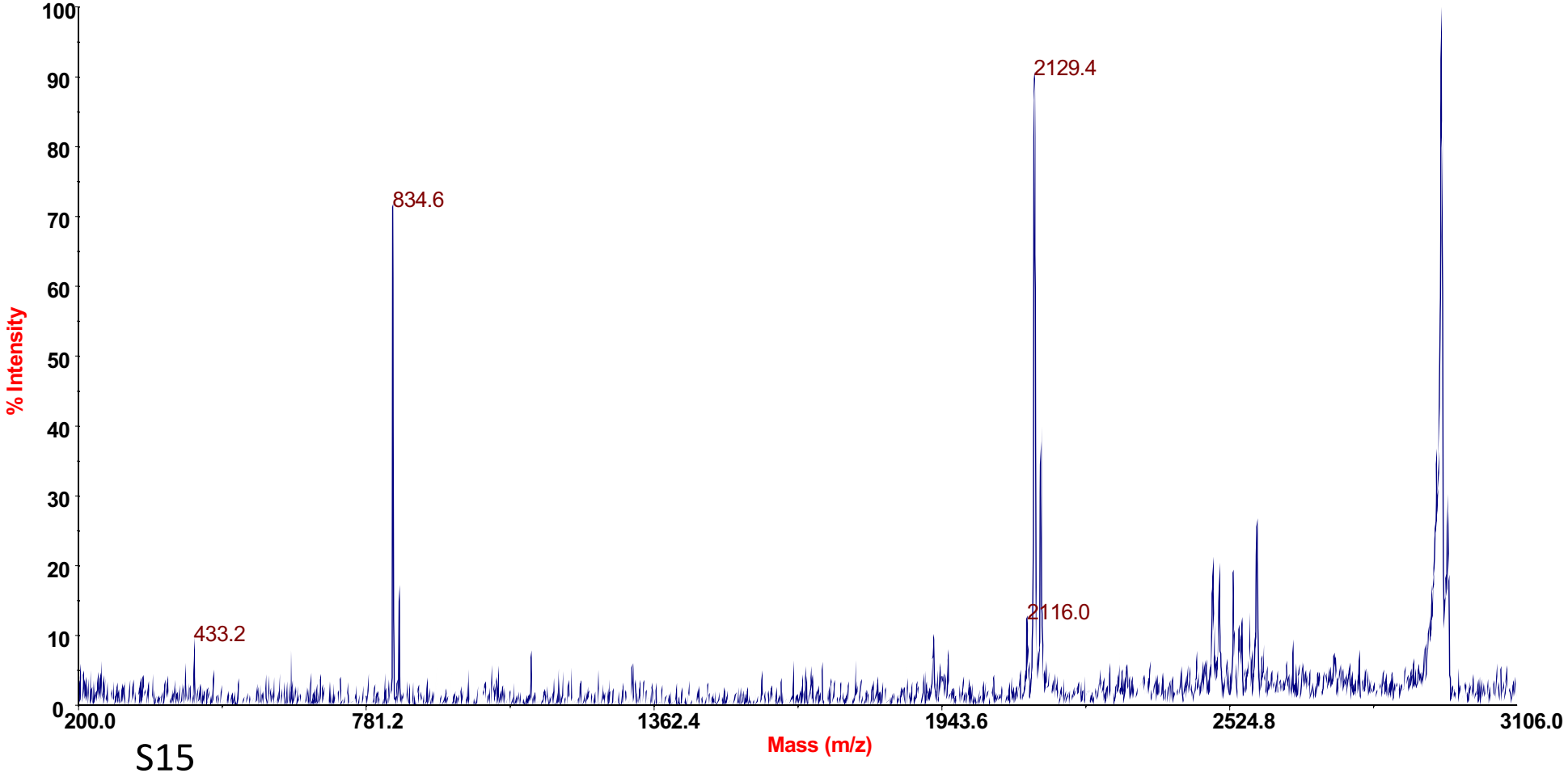
100
90
80
70
60
50
40
30
20
10
0
% Intensity
2129.4
834.6
433.2
2116.0
200.0
781.2
1362.4
1943.6
2524.8
3106.0
Mass (m/z)

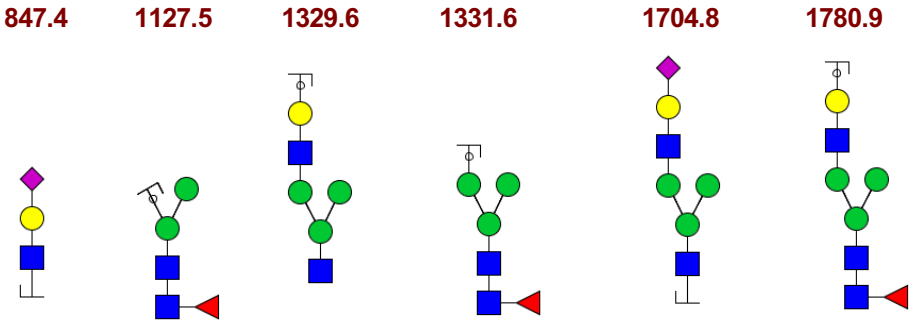
847.4
1127.5
1329.6
1331.6
1704.8
1780.9

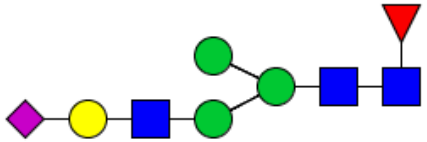

MS/MS 2156.1

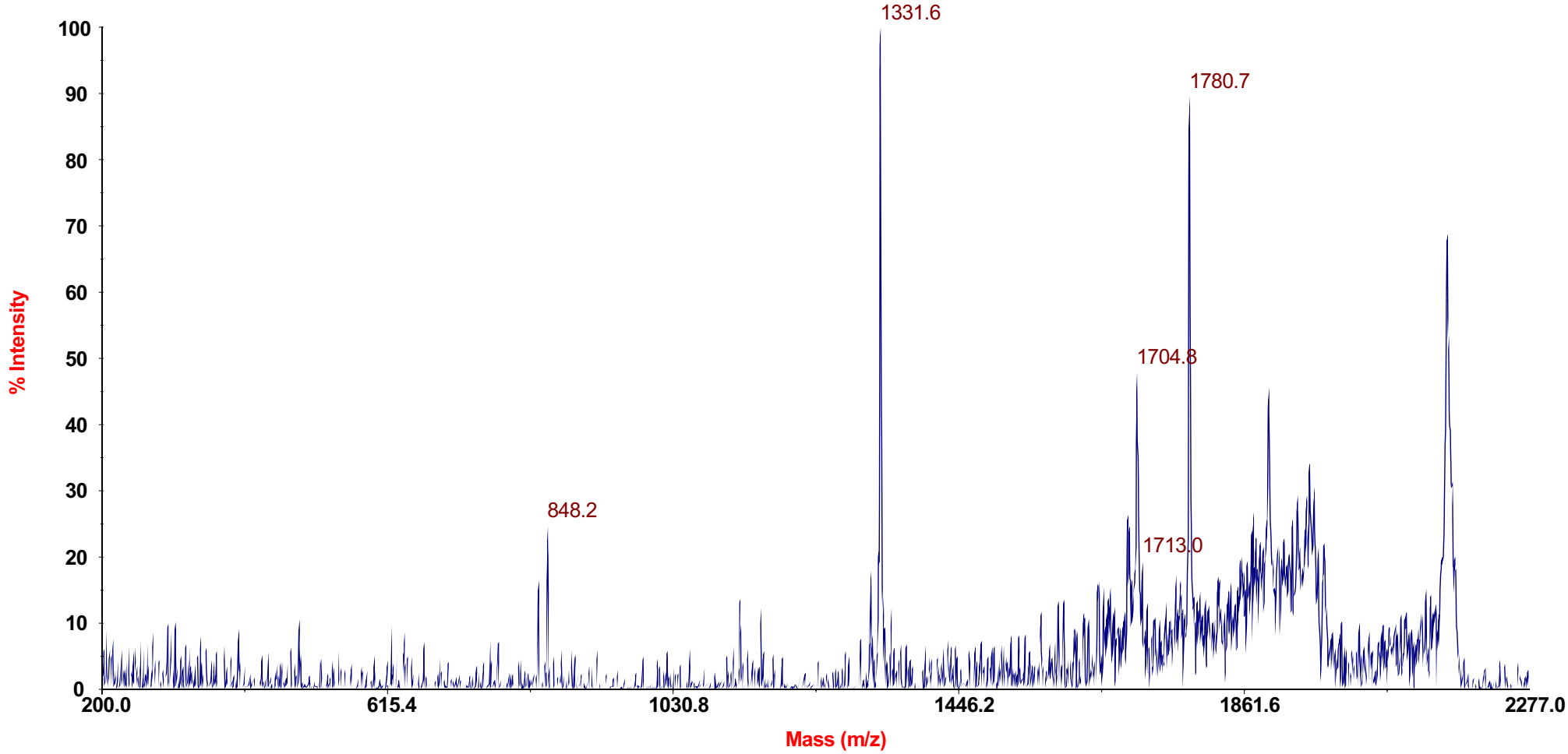
1331.6
1780.7
1704.8
848.2
1713.0
100
90
80
70
60
50
40
30
20
10
0
% Intensity
200.0
615.4
1030.8
1446.2
1861.6
2277.0
Mass (m/z)

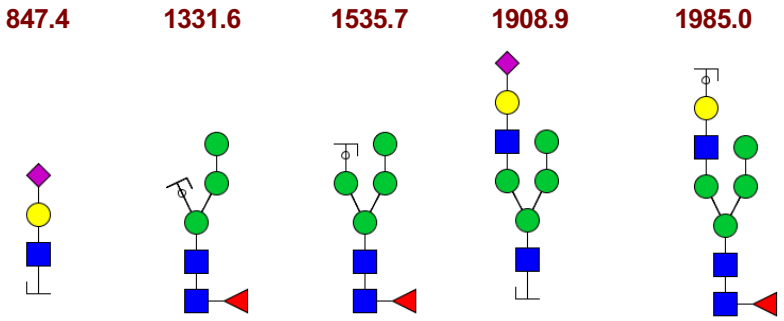
847.4
1331.6
1535.7
1908.9
1985.0

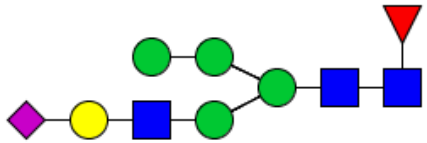

MS/MS 2360.2

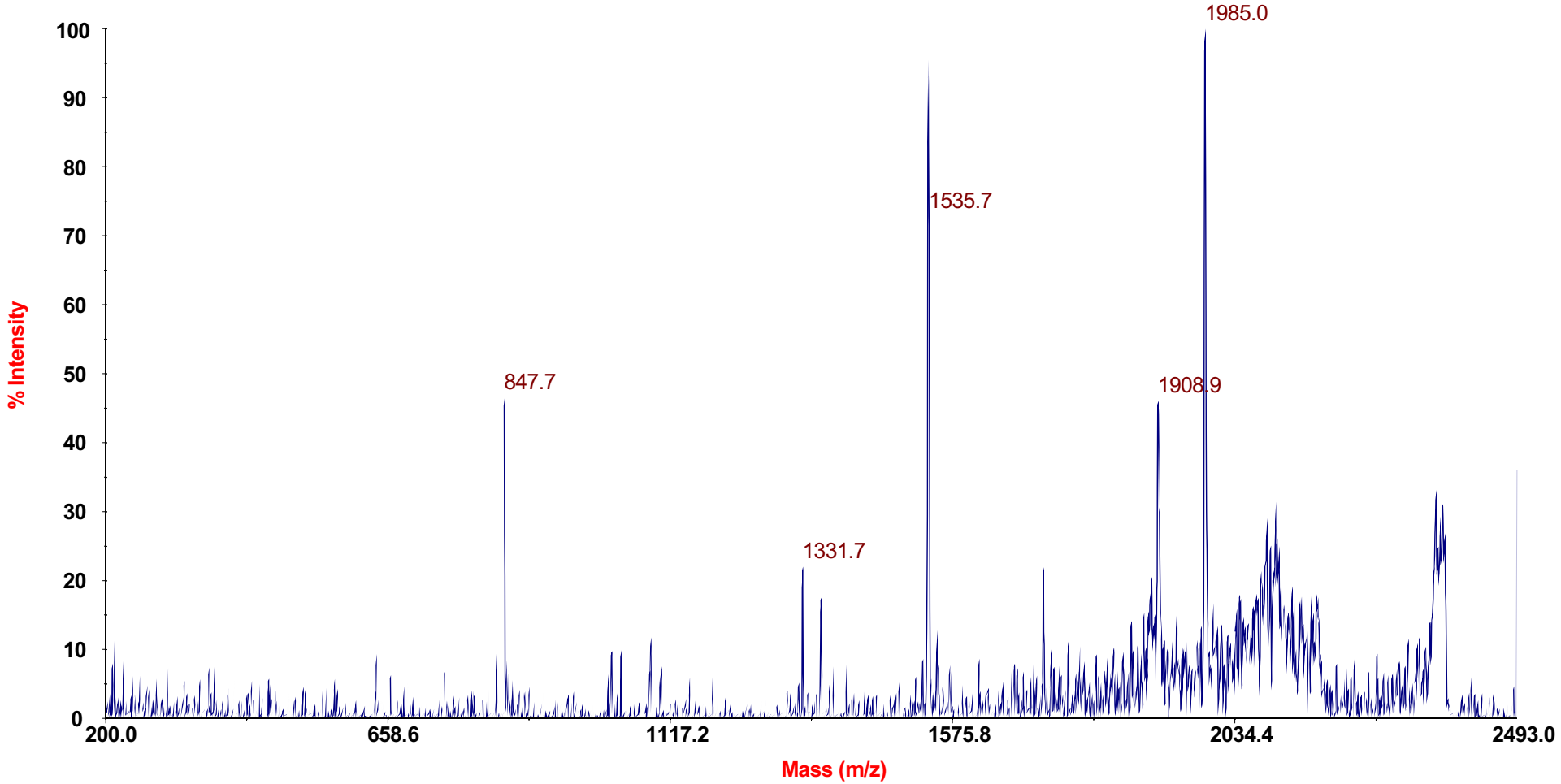
100
90
80
70
60
50
40
30
20
10
0
% Intensity
847.7
1331.7
1535.7
1908.9
1985.0
200.0
658.6
1117.2
1575.8
2034.4
2493.0
Mass (m/z)

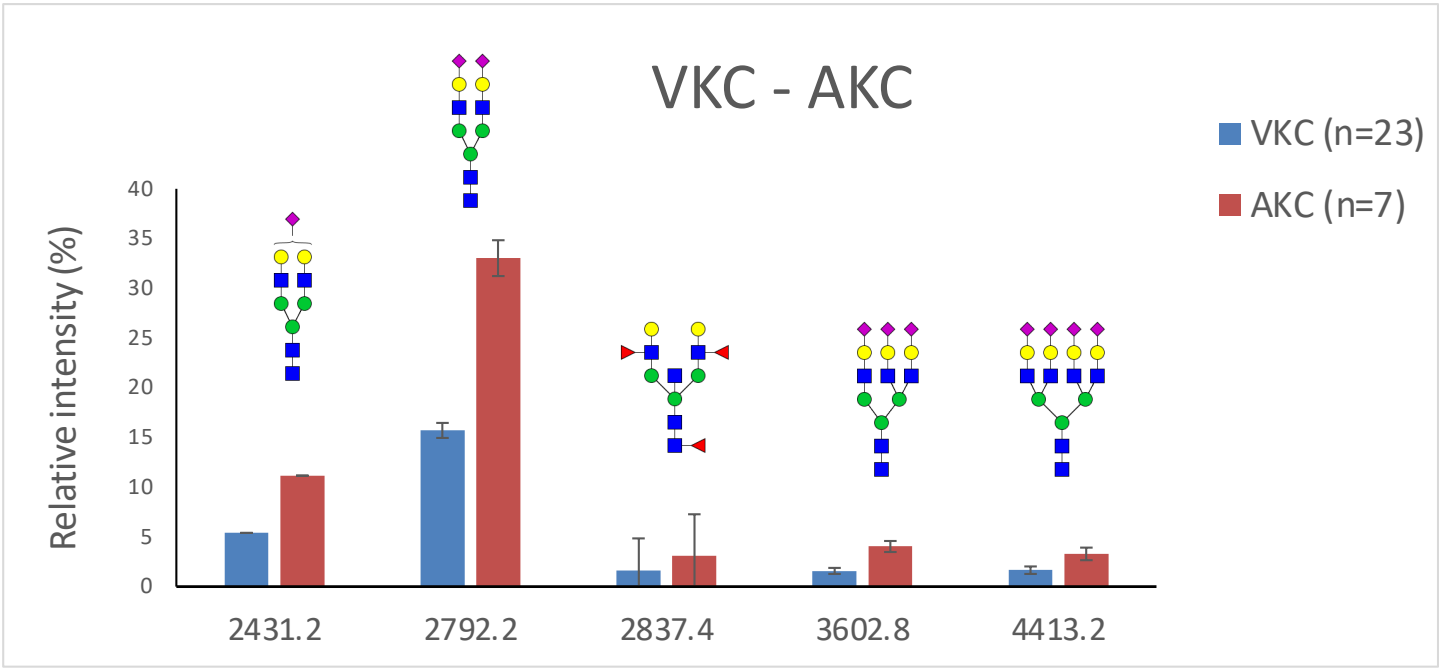
VKC - AKC
VKC (n=23)
AKC (n=7)
Relative intensity (%)
40
35
30
25
20
15
10
5
0
2431.2
2792.2
2837.4
3602.8
4413.2

S18